Paleoceanography and Paleoclimatology

RESEARCH ARTICLE
10.1029/2019PA003772

Key Points:
- The western equatorial Pacific was more saline than modern during the early Pliocene (5–3.6 Ma), consistent with an El Padre state
- In situ analyses of foraminifers improve the accuracy of salinity ($\delta^{18}O_{sw}$) reconstruction
- Trends in the in situ $\delta^{18}O_{sw}$ record are not apparent in the whole-shell record due to dissolution of primary foraminifer calcite

Supporting Information:
- Supporting Information S1
- Data Set S1
- Data Set S2
- Data Set S3
- Data Set S4
- Table S1
- Table S2
- Table S3
- Table S4

Correspondence to:
J. Wycech,
jody.wycech@colorado.edu

Citation:
Wycech, J., Kelly, D. C., Fournelle, J., Kitajima, K., Kozdon, R., & Orland, I. J. (2020). Reconstructing Pliocene west Pacific warm pool hydroclimate using in situ microanalyses on fossil planktic foraminifer shells. *Paleoceanography and Paleoclimatology*, *35*, e2019PA003772. https://doi.org/10.1029/2019PA003772

Received 29 SEP 2019
Accepted 24 APR 2020
Accepted article online 8 MAY 2020

Reconstructing Pliocene West Pacific Warm Pool Hydroclimate Using In Situ Microanalyses on Fossil Planktic Foraminifer Shells

J. Wycech[1,2], D. C. Kelly[1], J. Fournelle[1], K. Kitajima[1], R. Kozdon[3], and I. J. Orland[1]

[1]Department of Geoscience, University of Wisconsin-Madison, Madison, WI, USA, [2]Now at Cooperative Institute for Research in Environmental Sciences (CIRES) and Department of Geological Sciences, University of Colorado Boulder, Boulder, CO, USA, [3]Lamont-Doherty Earth Observatory of Columbia University, Palisades, NY, USA

Abstract A controversial aspect of Pliocene (5.3–2.6 Ma) climate is whether El Niño-like (El Padre) conditions, characterized by a reduced trans-equatorial sea-surface temperature (SST) gradient, prevailed across the Pacific. Evidence for El Padre is chiefly based on reconstructions of sea-surface conditions derived from the oxygen isotope ($\delta^{18}O$) and Mg/Ca compositions of shells belonging to the planktic foraminifer *Trilobatus sacculifer*. However, fossil shells of this species are a mixture of multiple carbonate phases—pre-gametogenic, gametogenic (reproductive), and diagenetic calcites—that formed under different physiological and/or environmental conditions and are averaged in conventional whole-shell analyses. Through in situ measurements of micrometer-scale domains within Pliocene-aged shells of *T. sacculifer* from Ocean Drilling Program Site 806 in the western equatorial Pacific, we show that the $\delta^{18}O$ of gametogenic calcite is 0.6–0.8‰ higher than pre-gametogenic calcite, while the Mg/Ca ratios of these two phases are the same. Both the whole-shell and pre-gametogenic Mg/Ca records indicate that average early Pliocene SSTs were ~1°C warmer than modern, with present-day SSTs being established during the latest Pliocene and early Pleistocene (~3.0–2.0 Ma). The measurement of multiple calcite phases by whole-shell $\delta^{18}O$ analyses masks a late Pliocene to earliest Pleistocene (3.6–2.2 Ma) decrease in seawater $\delta^{18}O$ ($\delta^{18}O_{sw}$) values reconstructed from in situ pre-gametogenic $\delta^{18}O$ and Mg/Ca measurements. Our novel $\delta^{18}O_{sw}$ record indicates that sea-surface salinities in the west Pacific warm pool were higher than modern prior to ~3.5 Ma, which is consistent with more arid conditions under an El Padre state.

Plain Language Summary The Pliocene (5.3–2.6 million years ago) is the most recent time in Earth history when atmospheric carbon dioxide concentrations may have been modern-like and the continents were in their current configuration. Thus, Pliocene climate reconstructions are considered a useful indicator of future conditions. Several Pliocene reconstructions from the equatorial Pacific argue for a sea-surface temperature distribution that resembles modern El Niño events. Relevant to this study, modern El Niño events also produce drier conditions in the western equatorial Pacific. We investigate Pliocene permanent El Niño, or El Padre, in the west Pacific by using paired oxygen isotope and Mg/Ca measurements of marine microfossils (foraminifera) to reconstruct the oxygen isotope composition of surface water ($\delta^{18}O_{sw}$), which tracks sea-surface salinity. In situ analyses were used to measure tiny spots within individual shells of *Trilobatus sacculifer* to target only domains formed near the sea surface. These measurements indicate that the early Pliocene west Pacific was drier than today, which is similar to modern El Niño events and consistent with El Padre. The in situ-based $\delta^{18}O_{sw}$ trend toward modern sea-surface salinities is not reconstructed by whole-shell measurements primarily due to the life cycle of *T. sacculifer*, which produces large oxygen isotope variability within individual shells.

1. Introduction

The Pliocene epoch (ca. 5.3–2.6 million years ago) is the most recent time in Earth history when global climate was appreciably warmer than the present and as such is considered an analog for climate conditions predicted for the latter part of this century (Crowley, 1996; Dowsett et al., 1996; Dowsett & Robinson, 2009). Added incentive for studying the Pliocene comes from geochemical evidence indicating that paleo-atmospheric CO_2 concentrations (350–450 ppmv) may have been comparable to those of the

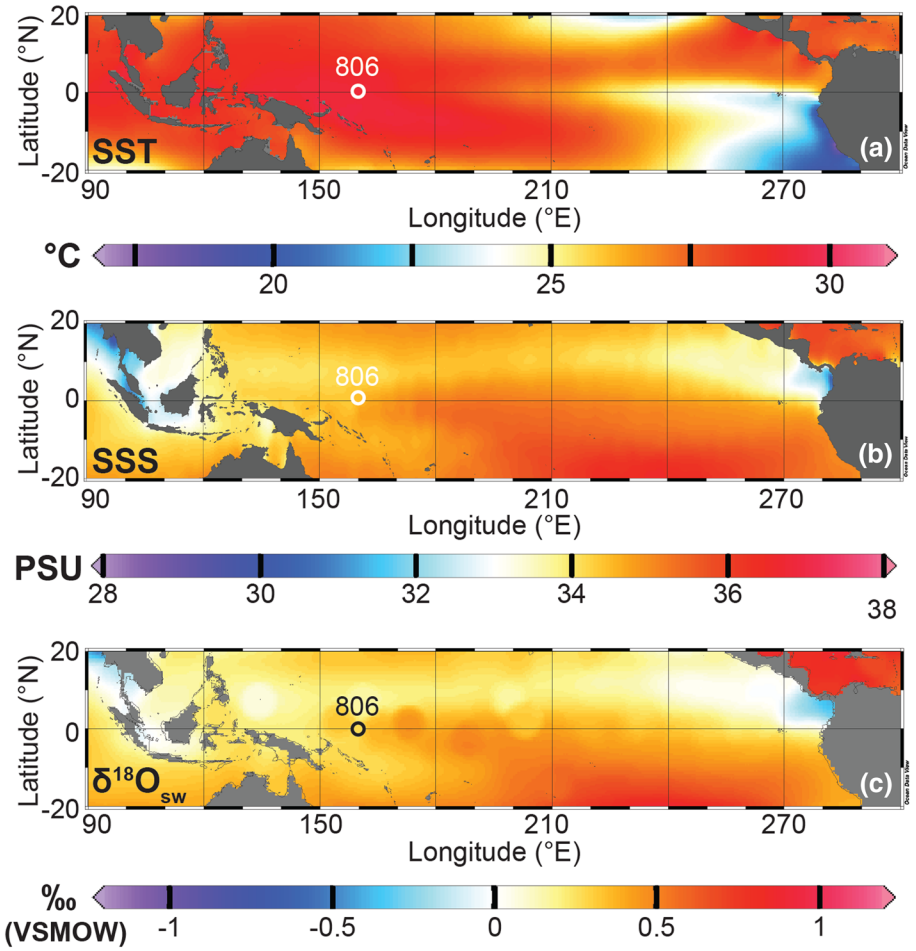

Figure 1. Location of Site 806 overlain on maps of modern equatorial Pacific showing observed (a) sea-surface temperatures (Locarnini et al., 2013), (b) sea-surface salinities (Locarnini et al., 2013), and (c) surface ocean $\delta^{18}O_{sw}$ values (Schmidt et al., 1999).

modern 400-ppm world (Pagani et al., 2010; Seki et al., 2010). A key component of the Pliocene ocean-climate system is the role that the hydrological cycle played in transferring tropical heat to extratropical regions under a warmer climate state. Specifically, the strength of Hadley Cell circulation is modulated by the balance between evaporation and precipitation along the equator (Wang, 2004; Xie, 2004). Thus, equatorial sea-surface temperatures (SSTs) and precipitation patterns have a global impact on the transport and redistribution of moisture (Bartoli et al., 2005; Krishna-Kumar et al., 2006; Ropelewski & Halpert, 1987, 1996), which plays an important role in balancing Earth's heat budget.

The redistribution of moisture in the modern equatorial Pacific is governed by Walker atmospheric circulation, which imparts an asymmetric zonal (E-W) precipitation gradient with wetter conditions in the west relative to the east (Bjerknes, 1969). However, several previous studies have posited that El Niño-like conditions, termed “El Padre” (Ravelo et al., 2014), prevailed across the equatorial Pacific during the early Pliocene as evidenced by a weakened zonal SST gradient and a deeper thermocline in the east Pacific (Cannariato & Ravelo, 1997; Chaisson & Ravelo, 2000; Dekens et al., 2008; Ford et al., 2015, 2012; Lawrence et al., 2006; Molnar & Cane, 2002; Philander & Fedorov, 2003; Ravelo et al., 2006; Seki et al., 2012; Wara et al., 2005; Wycech et al., 2019).

One approach to investigate El Padre and understand the hydroclimate state of the equatorial Pacific during the Pliocene is to reconstruct surface-ocean conditions at locations such as the west Pacific warm pool (WPWP) (Figure 1). Reconstruction of sea-surface salinity (SSS) through its paleoclimate proxy, the

oxygen isotope composition of seawater ($\delta^{18}O_{sw}$), is informative because these two seawater properties track each other and both are governed by spatiotemporal changes in evaporation and precipitation (Bigg & Rohling, 2000; Schmidt et al., 1999). In short, modern SSSs and surface-ocean $\delta^{18}O_{sw}$ values are low in wetter regions where precipitation exceeds evaporation because kinetic fractionation produces water vapor that is depleted in the heavier isotope (^{18}O) relative to the residual seawater (Figures 1b and 1c).

Most Pliocene climate reconstructions of SSTs and salinities ($\delta^{18}O_{sw}$) in the equatorial Pacific are derived from oxygen isotope ($\delta^{18}O$) and magnesium-calcium (Mg/Ca) ratios measured from planktic foraminifer shells. Culturing experiments on living foraminifers have shown that the $\delta^{18}O$ of their calcite is dependent upon both the calcification temperature and $\delta^{18}O_{sw}$ (Bemis et al., 1998; Erez & Luz, 1983), while the magnesium content of their shells increases exponentially with increasing temperatures (Lea et al., 1999; Nürnberg et al., 1996). Thus, the pairing of these two geochemical proxies can be used to reconstruct $\delta^{18}O_{sw}$ and SSS because Mg/Ca ratios provide an independent measure of SST (e.g., Groeneveld et al., 2014).

Although paired $\delta^{18}O$ and Mg/Ca measurements are theoretically useful, conventional measurements can be problematic because the fossil shells of many planktic foraminifer species are a mixture of three different carbonate phases—primary biogenic (PREGAM), reproductive gametogenic (GAM), and secondary diagenetic calcites—that each formed under disparate environmental and physiological conditions (Bé, 1980; Killingley, 1983; Schiebel & Hemleben, 2005). The addition of GAM and diagenetic calcites poses a major problem for reconstructing tropical SST and $\delta^{18}O_{sw}$ records because these carbonate phases typically form at colder deep-water temperatures (Duplessy et al., 1981; Schrag et al., 1995) and on micrometer scales (e.g., Groeneveld et al., 2008) that are too small to be separately analyzed with conventional techniques. To complicate matters, conventional analyses do not capture inter-shell variability within a given sample because they typically require multiple whole shells for a single analysis.

Here, we use microanalytical techniques such as secondary ion mass spectrometry (SIMS) and electron probe microanalysis (EPMA) to perform isolated measurements on different domains within an individual shell. These in situ techniques provide a means for disentangling the geochemical signals of different carbonate phases and, as such, hold much promise for enhancing our understanding of how secondary processes such as gametogenesis and diagenesis influence the primary paleoclimate signals encoded in fossil planktic foraminifer shells. SIMS measures the $\delta^{18}O$ composition of foraminifer calcite by targeting 3- to 10-μm-diameter domains within an individual shell, whereas EPMA measures the Mg/Ca ratio of foraminifer calcite from 2-μm domains within an individual shell. The ultra-high spatial resolution of these in situ measurements can be used to distinguish between the primary and secondary calcite phases (Kozdon et al., 2013; Wycech, Kelly, Kitajima, et al., 2018). Relative to whole-shell measurements, the pairing of in situ $\delta^{18}O$ and Mg/Ca analyses promises more accurate SST and $\delta^{18}O_{sw}$ reconstructions by targeting only PREGAM calcite that formed within the oceanic mixed layer (euphotic zone) in the same shell. Thus, in situ techniques eliminate signal-averaging effects that can obscure important trends in paleoclimate records constructed with conventional whole-shell analyses. Here, we use $\delta^{18}O$ and Mg/Ca in situ measurements of PREGAM calcite domains in individual shells of the planktic foraminifer, *Trilobatus sacculifer*, to reconstruct Pliocene SST and $\delta^{18}O_{sw}$ values in the WPWP and test for high-$\delta^{18}O_{sw}$ El Padre signatures (sensu Ravelo et al., 2006).

2. Materials and Methods

2.1. Study Site and Core Sampling

Ocean Drilling Program (ODP) Site 806 is located atop the Ontong Java Plateau (0°19.11′N, 159°21.69′E; 2,520-m water depth) in the western equatorial Pacific (Shipboard Party, 1991; Figure 1) and is well positioned for detecting changes in Pliocene Walker Circulation (Ravelo et al., 2006). The Site 806 Pliocene section has been constrained by biostratigraphic and astrochronological methodologies (Jansen et al., 1993), which served as guide for sample selection. Accordingly, a stratigraphic series comprising 22 core samples was taken from the Plio-Pleistocene section (5.1–2.2 Ma) of Site 806, Hole B. The temporal resolution used by previous studies (~10 kyr) is impractical for this study owing to the labor-intensive nature of sample preparation required for in situ measurements and the need for numerous in situ measurements within an

individual planktic foraminifer shell. For this reason, the records herein reported span 5.1–2.2 Ma with a sampling resolution varying between 40 and 260 kyr (mean = 139 kyr). Each core sample was disaggregated using a pH-buffered sodium hexametaphosphate hydrogen peroxide (30%$_v$) solution, wet sieved (>63 μm), rinsed with distilled water, and oven-dried at 30°C overnight.

Shells of the mixed-layer dwelling planktic foraminifer species, *T. sacculifer*, were handpicked from the 355- to 425-μm size fraction. We targeted *T. sacculifer* for study because (1) numerous field and culturing studies have calibrated the $\delta^{18}O$ and Mg/Ca ratios of this species against temperature (Anand et al., 2003; Dekens et al., 2002; Elderfield & Ganssen, 2000; Erez & Luz, 1983; Mulitza et al., 2003; Nürnberg et al., 1996; Regenberg et al., 2009; Rosenthal et al., 2000; Spero et al., 2003), (2) *T. sacculifer* has a continuous fossil record through the study section, (3) it is commonly used for equatorial Pliocene sea-surface reconstructions (e.g., Billups et al., 2007; Groeneveld, 2005), and (4) whole-shell *T. sacculifer* $\delta^{18}O$ and Mg/Ca records for the Site 806 Pliocene section have been previously published (Wara et al., 2005).

2.2. Specimen Preparation and In Situ Measurements

Prior to cross-sectioning for in situ analysis, we acquired back-scatter electron (BSE) scanning electron microscope (SEM) images showing the exteriors of most *T. sacculifer* shells (supporting information Data Set S1). These images were obtained using a Hitachi S-3400N SEM in variable pressure mode. The *T. sacculifer* shells and three grains of the UWC-3 calcite standard ($\delta^{18}O = -17.9‰$ VPDB; 5,450-ppm Mg; Kozdon et al., 2009) were placed within a 5-mm-diameter circular area and cast in a 25-mm-diameter epoxy mount. The mount was then ground to level of best exposure in cross-section, polished with carbonate-epoxy relief of less than ~1 μm (Kita et al., 2009), and gold coated. Secondary electron (SE) SEM images of each mounted shell were subsequently taken in high vacuum mode to assess specimen exposure quality and cross-section geometry prior to in situ analysis (Data Set S2).

In situ measurements were generally taken from the penultimate (f-1) chamber where the shell wall was thickest and composed of both PREGAM and GAM calcites. The ultimate (f) chamber was not typically analyzed because the PREGAM and GAM calcites were indistinguishable under SEM and the chamber is known to have a lower Mg/Ca ratio than the other chambers (Sadekov et al., 2005), which indicates that it forms in deeper water (Sadekov et al., 2009). The $\delta^{18}O$ values of individual *T. sacculifer* chambers are statistically indistinguishable from one another (Spero & Lea, 1993), so SIMS analysis of the penultimate chamber is representative of the other chambers. In rare instances, in situ analyses were performed on ultimate (f) and anti-penultimate (f-2) chambers due to porous PREGAM or thin GAM domains in the penultimate chamber. Multiple in situ measurements were taken from both the PREGAM and GAM calcites of each shell, with average $\delta^{18}O_{calcite}$ values and Mg/Ca ratios of the two calcite phases being calculated per shell from these individual measurements. These average shell values were then used to calculate the average PREGAM and GAM $\delta^{18}O_{calcite}$ or Mg/Ca ratio for a sample as well as inter-shell $\delta^{18}O_{calcite}$ and Mg/Ca variability (±2 SE). Thus, in situ measurements capture both intra- and inter-shell geochemical variability of a given sample. Although in situ measurement entails analysis of fewer shells relative to the conventional whole-shell technique, the accuracy of the reconstruction is improved by targeting only the PREGAM calcite. Our approach is particularly well suited at Site 806 where seasonality is low, and fewer shells are required for a representative sample of environmental conditions relative to high-latitude sites.

2.2.1. SIMS $\delta^{18}O$ Measurements

In situ $\delta^{18}O$ analyses were performed with a CAMECA IMS 1280 ion microprobe at the WiscSIMS Laboratory, Department of Geoscience, University of Wisconsin-Madison, using a $^{133}Cs^+$ primary ion beam and previously reported conditions (Kita et al., 2009; Kozdon et al., 2013; Valley & Kita, 2009). Each series of 8–12 spot $\delta^{18}O$ measurements carried out on foraminifer calcite was bracketed by 4–6 consecutive analyses of $\delta^{18}O$ in a grain of UWC-3 calcite running standard (Kozdon et al., 2009) mounted in the center of the sample mount. We standardized the measurements using these bracketing standard analyses to determine instrumental mass fractionation corrections for each set of foraminifer calcite measurements and reported the $\delta^{18}O$ values relative to VPDB.

Measurements from ~10-μm spot sizes (1–2 μm deep) were obtained with an average ion beam intensity of 0.99 nA. The 10-μm spots were used to obtain numerous, precise intra-shell $\delta^{18}O$ values from both

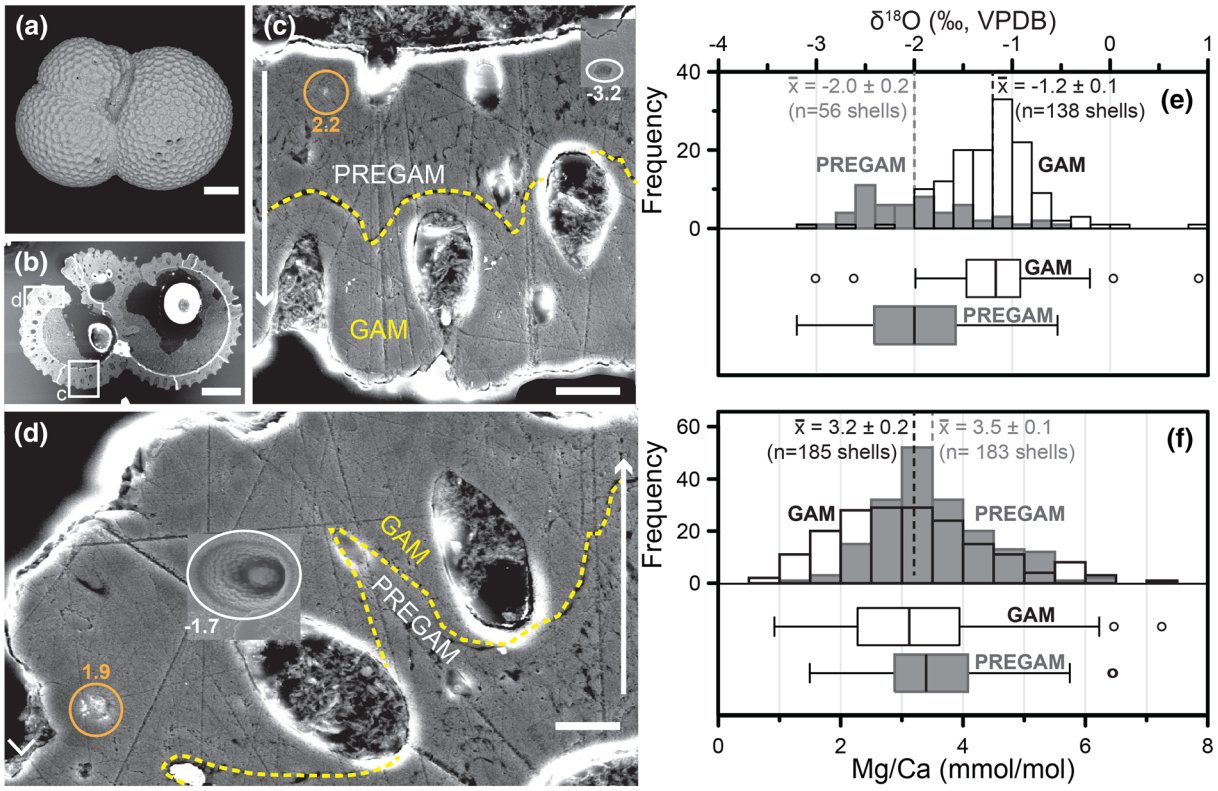

Figure 2. Images of representative *Trilobatus sacculifer* shell showing locations of in situ microanalyses, and distributions of resulting geochemical data compiled from the Site 806 Pliocene shells. (a) Back-scatter electron SEM image of *T. sacculifer* shell (SIMS Mount WP7, Shell 90, Site 806, Hole B, Core 6, section 5, 88–89 cm) showing shell exterior. (b) Secondary electron (SE) SEM image of cross-section through shell shown in panel (a) mounted in epoxy. Scale bars in panels (a) and (b) are 100 μm. (c and d) Highly magnified SE SEM image of cross-section through penultimate chamber (see boxes in (b)) showing SIMS and EPMA spots with respective $\delta^{18}O$ values (white, ‰ measured) and Mg/Ca ratios (orange, mmol/mol). White arrows indicate direction of chamber growth with GAM crust coating shell exterior delimited by yellow dashed line. Scale bars are 10 μm. (e and f) Overlapping histograms (upper panels) with box and whisker plots (lower panels) showing distributions of per-shell average in situ $\delta^{18}O_{calcite}$ values and Mg/Ca ratios measured from PREGAM (gray) and GAM (translucent white) calcites of *T. sacculifer*. Median and mean values (±2 SE) denoted by solid vertical lines within boxes and dashed vertical lines, respectively. Whiskers on boxes are 1.5 times the interquartile range. Outliers are small circles outside of whiskers.

the PREGAM and GAM calcites (Figures 2a–2d). Secondary $^{18}O^-$, $^{16}O^-$, and $^{16}OH^-$ ions were detected from the 10-μm spots using three Faraday cup detectors with a typical $^{16}O^-$ count rate of 1.9×10^9 counts per second (cps). The total analytical time per spot was ~3 min including pre-sputtering. The average precision, as determined from the sets of bracketing UWC-3 standard measurements, was ±0.3‰ (2 standard deviation [SD], spot-to-spot). A total of 518 10-μm SIMS $\delta^{18}O$ measurements was performed on *T. sacculifer* shells in addition to 222 bracketing measurements of the UWC-3 standard (Table S1).

A second analytical setup with an ion beam current of 14 pA and a spot size of ~3 μm was used to measure unusually small (<10 μm diameter) PREGAM domains. Secondary $^{18}O^-$ and $^{16}O^-$ ions were detected simultaneously using a Faraday cup ($^{16}O^-$) and an electron multiplier ($^{18}O^-$) with a typical $^{16}O^-$ count rate of 3.1×10^7 cps. Secondary $^{16}OH^-$ ions were detected using a Faraday cup. During the session in 2014, the applied high voltage to the electron multiplier was manually checked and increased as needed after each bracket at a rate of 2–3 V/hr to compensate for drift in the electron multiplier gain. The electron multiplier was automatically checked and adjusted after every analysis during the 2017 session. The total analytical time per spot was 7 min including pre-sputtering. The average precision for the 3-μm analyses, as determined from the sets of bracketing standard measurements, was ±0.7‰ (2 SD, spot-to-spot). A total of 84 3-μm SIMS $\delta^{18}O$ measurements was performed on *T. sacculifer* shells in addition to 72 bracketing measurements of the UWC-3 standard.

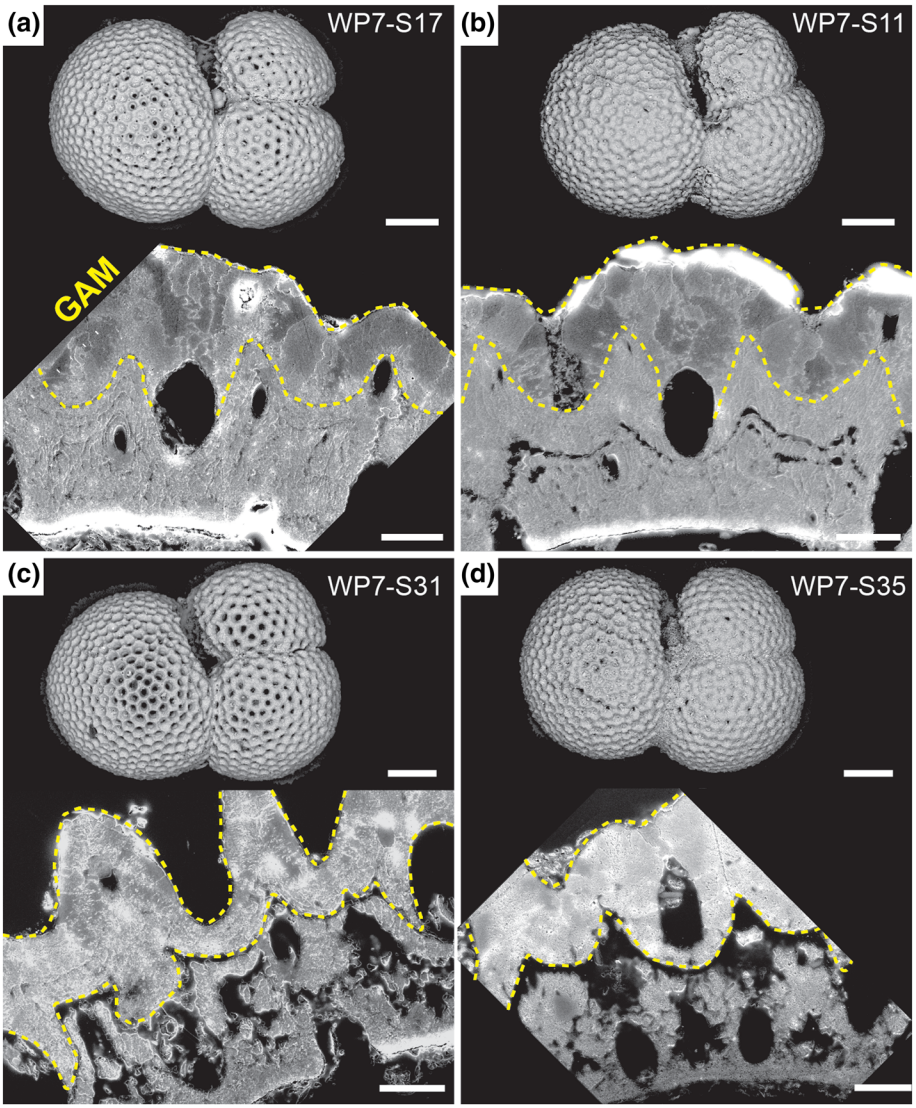

Figure 3. Comparison of external and internal preservation of Pliocene-aged *Trilobatus sacculifer* shells from Site 806. (a–d) BSE SEM images of whole-shell exteriors (upper panels) with highly magnified SE SEM images of penultimate chamber in cross-section (lower panels). Note similar external wall textures of whole shells, but disparate preservation of PREGAM calcite and varying proportions of GAM crust (yellow dashed line). Scale bars are 100 μm for whole-shell images, 10 μm for chamber wall cross-sections. Specimen number in upper right of each panel. Note that PREGAM calcite analyses by SIMS and EPMA were not performed on specimens shown in panels (c) and (d) due to lack of suitable domains.

Following SIMS $\delta^{18}O$ analyses, each analysis spot was imaged by SEM using the SE detector in high vacuum mode (Data Set S3). Individual measurements on *T. sacculifer* shells were assessed based on the visual appearance of the analysis pits as well as the $^{16}O^-$ ion yield and count rate relative to the standard (see section S1). SIMS $\delta^{18}O$ values were measured from PREGAM calcite (1–3 pits per shell) and GAM calcite (1–3 pits per shell). Although numerous (10–30) *T. sacculifer* shells from each core sample were prepared for in situ analysis, many of the shells were not analyzed due to poor preservation of the PREGAM calcite (Figure 3). As a result, the SIMS analyses yielded successful PREGAM and GAM measurements from an average of 3 and 6 shells per sample, respectively. PREGAM calcite was successfully analyzed by SIMS in only 18 out of the 22 targeted samples due to varying degrees of dissolution of this calcite phase over several stratigraphic intervals. In 6 of these 18 samples, the PREGAM calcite $\delta^{18}O$ value was successfully measured from only 1 shell per sample.

Previous comparison of $\delta^{18}O_{calcite}$ values obtained by conventional gas-source mass spectrometry (GSMS) and SIMS revealed an inter-instrumental difference where $\delta^{18}O$ values measured by 10- and 3-μm SIMS pits were 0.9 ± 0.1‰ lower than paired GSMS values measured from the same chamber of core-top and cultured shells of *Orbulina universa*, a foraminifer with an ecology similar to that of *T. sacculifer* (Wycech, Kelly, Kozdon, et al., 2018). Application of this adjustment (+0.9‰) to SIMS $\delta^{18}O$ values measured from *T. sacculifer* shells was deemed appropriate in a subsequent study carried out on Holocene-aged specimens taken from core-top samples (Wycech, Kelly, Kitajima, et al., 2018). In this study, the applicability of such an adjustment is further assessed by using the $^{16}OH/^{16}O$ (OH/O herein) ratios measured by SIMS. The OH/O ratios are thought to reflect the amount of water or organic matter bound within the matrix of foraminifer calcite (Wycech, Kelly, Kozdon, et al., 2018) and serve as a qualitative indicator of measured phases that may partly contribute to the SIMS-GSMS $\delta^{18}O$ difference. Even at ultra-high vacuum, the SIMS analytical chamber contains detectable hydrous compounds, so the reported OH/O ratios were background-corrected by subtracting the average OH/O of the UWC-3 (nominally anhydrous metamorphic calcite) bracketing data from the OH/O ratio of the foraminifer. The average background-corrected OH/O ratios of the Pliocene-aged *T. sacculifer* shells are within 2 SD of the average OH/O ratios of the *O. universa* shells (Wycech, Kelly, Kozdon, et al., 2018; see Figure S1), which suggests that the organic or water content of the calcite composing *T. sacculifer* shells is comparable to that of the calcite composing Holocene-aged *O. universa* shells. Thus, the SIMS $\delta^{18}O$ adjustment determined from *O. universa* measurements is deemed appropriate for the SIMS measurements obtained from *T. sacculifer* shells in this study. An adjustment of +0.9‰ is hereafter applied to all SIMS $\delta^{18}O$ values measured from specimens of *T. sacculifer*. All unadjusted and adjusted SIMS $\delta^{18}O$ values are reported in Table S1.

2.2.2. EPMA Mg/Ca Measurement

EPMA provides accurate measurements of the minor and trace element compositions of planktic foraminifer calcite at micrometer scales (Brown & Elderfield, 1996; Elderfield & Ganssen, 2000; Fehrenbacher & Martin, 2010, 2014; Lipps & Ribbe, 1967; Nürnberg et al., 1996; Sadekov et al., 2005). In this study, the Mg/Ca ratios of the *T. sacculifer* shells were analyzed from ~2-μm domains (Figures 2a–2d) using the CAMECA SX51 electron microprobe at the University of Wisconsin-Madison Department of Geoscience. Quantitative analyses, including mineral standard measurement, background subtraction, and matrix correction, were performed using Probe for EPMA© software. Measurements were made using an accelerating voltage of 15 kV, a 10-nA Faraday current, and a focused beam with a counting time of 20 s on the peak and 10 s on each of the two background positions. The natural carbonate standards Delight Dolomite and UWC-3 were used for Ca and Mg. Mg Kα X-rays were measured by two TAP spectrometers and aggregated. Ca X-rays were measured by two PET spectrometers and aggregated. Carbon was calculated in the matrix correction atomically as C = (Ca + Mg + Sr). Analyses were performed using the "Time Dependent Intensity" feature of Probe for EPMA software which determines the elemental count rate by measuring Ca and Mg in 4-s increments, plotting the counts over time, and extrapolating back to the start time ($t = 0$ s). The quality of Mg/Ca ratio measurements was assessed on a session-by-session basis using the elemental totals and pit appearances (see section S2 and Figure S2). The targeted domains were subsequently imaged by SEM with the secondary electron detector after the EPMA session to identify the measured calcite phase (Data Set S4).

EPMA Mg/Ca ratios were collected from the PREGAM (~3 pits per shell) and GAM (~2 pits per shell) calcites of the mounted Pliocene and core-top *T. sacculifer* shells. An average of 8 shells were measured from each sample. Large intra-shell Mg/Ca ratio variability (up to 10 mmol/mol) has been measured for symbiont-bearing foraminifera including *T. sacculifer* (Eggins et al., 2004). However, the EPMA interaction volume of ~6 μm^3 and multiple analyses per domain provides for optimal determination of the average Mg/Ca ratios for PREGAM and GAM calcites in each shell. These average shell Mg/Ca ratios were then used to calculate the average PREGAM and GAM Mg/Ca ratios per sample. A total of 1,100 Mg/Ca ratios was collected by EPMA and is listed in Table S2.

2.3. Calculation of Pliocene SSTs

Measured in situ PREGAM and published whole-shell Mg/Ca ratios are used to calculate Pliocene SSTs with the Dekens et al. (2002) Mg/Ca-temperature calibration (Table S3). This Mg/Ca-temperature calibration includes a dissolution correction based on core depth that is deemed appropriate for SST reconstruction at

Site 806 because many of the *T. sacculifer* shells examined have partially dissolved PREGAM domains (Figure 3 and Data Set S2; Wycech, Kelly, Kitajima, et al., 2018). In addition, our SST calculations include a correction for lower Mg/Ca ratios of Pliocene seawater (Mg/Ca_{sw}) provided by Zeebe and Tyrrell (2019). The correction for lower Mg/Ca_{sw} entailed multiplying the Mg/Ca-temperature pre-exponential constant by the ratio of Pliocene/modern Mg/Ca_{sw} (sensu Medina-Elizalde et al., 2008) where modern Mg/Ca_{sw} is 5.17 mol/mol (Rausch et al., 2012). Thus, our approach to calculating Pliocene SSTs accounts for partial dissolution (etching) of the PREGAM calcite and secular variation in Mg/Ca_{sw}.

2.4. Calculation of Pliocene Surface-Ocean $\delta^{18}O_{sw}$ Values

For comparative purposes, two surface-ocean $\delta^{18}O_{sw}$ records were reconstructed by pairing the SSTs reconstructed from whole-shell Mg/Ca ratios with $\delta^{18}O$ values measured from either in situ PREGAM calcite (this study) or the whole-shell conventional technique (Wara et al., 2005). The use of the whole-shell SSTs in both $\delta^{18}O_{sw}$ calculations illustrates the effect of in situ versus whole-shell $\delta^{18}O$ measurements on the resulting $\delta^{18}O_{sw}$ values.

The average PREGAM-based $\delta^{18}O_{sw}$ value of each sample was used to construct the $\delta^{18}O_{sw}$ time series (Table S3). The Pliocene surface-ocean $\delta^{18}O_{sw}$ values are compared to the modern observed $\delta^{18}O_{sw}$ at Site 806 after adjusting for the difference in ice volume. This ice-volume correction (IVC) was computed with the simple assumption that global sea level tracks global ice volume and $\delta^{18}O_{sw}$; that is, a sea level rise of 10 m in the Pliocene equates to a 0.055‰ decrease in global $\delta^{18}O_{sw}$ during warm, pre-Pleistocene time periods (Miller et al., 1987). Most sea level records suggest that Pliocene sea level was 0–25 m higher than modern (Dwyer & Chandler, 2009; Krantz, 1991; Wardlaw & Quinn, 1991), which provided the required IVC (0 to −0.14‰) to raw $\delta^{18}O_{sw}$ values. The maximum sea level range reported for the Pliocene (0–40 m; Dwyer & Chandler, 2009; Krantz, 1991; Wardlaw & Quinn, 1991) provided the IVC extremes (0 to −0.22‰ adjustment) and a maximum envelope of uncertainty on the average IVC $\delta^{18}O_{sw}$ record.

The error on the whole-shell and in situ $\delta^{18}O_{sw}$ records was propagated with 1.2°C SST uncertainty (Anand et al., 2003; Dekens et al., 2002; Lea et al., 1999) and $\delta^{18}O$ error of either 0.1‰ from whole-shell measurements or 0.2–0.8‰ propagated from in situ PREGAM calcite measurements (see section S3 for more details). The resulting error on the $\delta^{18}O_{sw}$ reconstructions was 0.3‰ for the whole-shell record and 0.3–0.8‰ for the PREGAM record.

3. Results

3.1. PREGAM and GAM Calcite $\delta^{18}O$ and Mg/Ca Compositions

SIMS analysis of Pliocene-aged shells from Site 806 confirms that the whole-shell $\delta^{18}O$ composition of *T. sacculifer* is an aggregate mixture of at least two phases of calcite that have different $\delta^{18}O_{calcite}$ signatures. Specifically, GAM calcite has $\delta^{18}O$ values that, on average, are 0.8‰ higher than those of PREGAM calcite (Figure 2e). This result is consistent with in situ $\delta^{18}O$ measurements of *T. sacculifer* shells recovered from core-top (Holocene) samples (Wycech, Kelly, Kitajima, et al., 2018) and supports the inferred presence of a high-$\delta^{18}O$ GAM calcite phase on *T. sacculifer* shells posited by earlier studies (e.g., Duplessy et al., 1981). By contrast, the PREGAM Mg/Ca ratios are, on average, only 0.3 mmol/mol higher than the GAM Mg/Ca ratios of the same *T. sacculifer* shells from Site 806 (Figure 2f). Although this result is incongruous with in situ measurements of Mg/Ca ratios in cultured *T. sacculifer* (Nürnberg et al., 1996), it is consistent with previously published spatial maps of Mg/Ca ratios in *T. sacculifer* shells taken from core-top samples (Sadekov et al., 2005).

3.2. Core-Top $\delta^{18}O_{sw}$ Reconstruction

We assess the accuracy of our methods by comparing the modern SST and $\delta^{18}O_{sw}$ values observed at Site 806 to those reconstructed from paired $\delta^{18}O$ and Mg/Ca measurements of *T. sacculifer* shells taken from the core top sample (Figure 4). Similar to the Pliocene $\delta^{18}O$ data (Figure 2e), the average $\delta^{18}O$ values for the GAM calcite of the Holocene-aged *T. sacculifer* shells are 1.4‰ higher than the average $\delta^{18}O$ value of PREGAM calcite (Figure 4a) with the previously published whole-shell $\delta^{18}O$ value (Wara et al., 2005) falling between the mean PREGAM and GAM $\delta^{18}O$ values.

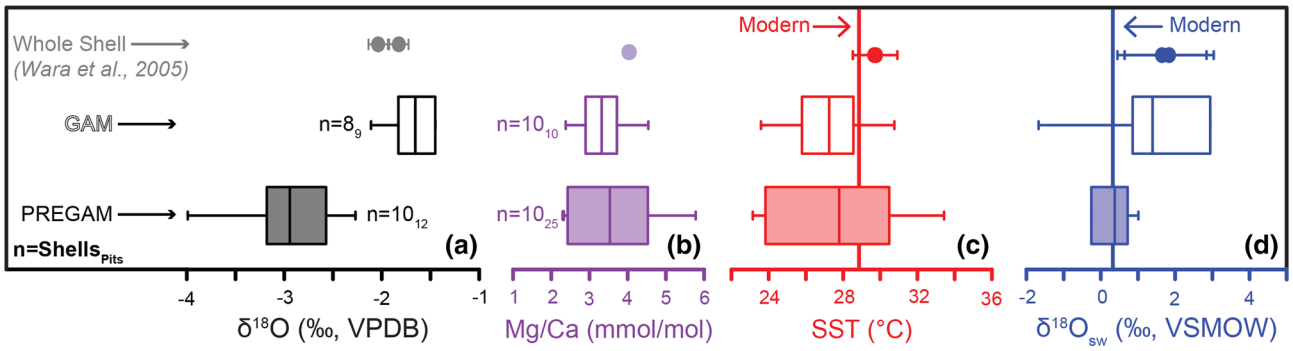

Figure 4. Comparison of in situ values (this study) to published whole-shell (Wara et al., 2005) $\delta^{18}O$ and Mg/Ca ratios for Holocene-aged *Trilobatus sacculifer* shells from Site 806 core-top (0–2 cm), and comparison of calculated SSTs and $\delta^{18}O_{sw}$ values to those observed (modern) at Site 806. (a–d) Box and whisker plots of in situ and reconstructed values from PREGAM calcite (colored boxes), GAM calcite (white boxes), and whole shells (filled circles). In situ data sets consist of per-shell averages, with median values denoted by solid vertical lines within boxes. Whiskers on boxes are 1.5 times the interquartile range. Number of shells and pits analyzed noted by "n" for in situ measurements. (a) Plots of measured $\delta^{18}O$ values. Whole-shell values (−2.0‰ and −1.8‰, VPDB) with analytical precision error (±0.1‰). (b) Plots of measured Mg/Ca ratios (whole-shell Mg/Ca ratios = 4.1 and 4.0 mmol/mol). (c) Plots of Mg/Ca-based and observed SSTs. Error on whole-shell SST = 1.2°C (Anand et al., 2003; Dekens et al., 2002; Lea et al., 1999). Modern SST (28.9°C, NOAA/TAO) denoted by vertical line. (d) Plots of calculated and observed $\delta^{18}O_{sw}$ values. Error on whole-shell $\delta^{18}O_{sw}$ = 1.2‰ (Rohling, 2000; Schmidt, 1999). Modern surface-ocean $\delta^{18}O_{sw}$ at Site 806 (0.3‰, VSMOW) denoted by vertical line (Schmidt et al., 1999).

By contrast, the average Mg/Ca ratios for the GAM calcite of the core-top *T. sacculifer* shells are statistically indistinguishable from the average Mg/Ca ratios of the PREGAM calcite (Figure 4b). The PREGAM and GAM Mg/Ca ratios of shells from the core-top sample exhibit large inter-shell variability (3.5 and 4.5 mmol/mol ranges, respectively), which is not captured by pooled, multi-shell Mg/Ca measurements. The whole-shell Mg/Ca ratios for Site 806 shells are 0.4–0.8 mmol/mol higher than the average PREGAM and GAM calcite Mg/Ca ratios but are still within 1 SD of the in situ Mg/Ca ratios.

The SSTs reconstructed for the core-top sample reflect the similarity between the in situ and whole-shell Mg/Ca ratios (Figure 4c). Specifically, the PREGAM-, GAM-, and whole-shell-derived SSTs all successfully reconstruct the modern mean annual temperature (28.9°C, NOAA/TAO) observed over the range of water depths (0- to 100-m water depths) inhabited by *T. sacculifer*. The average GAM-derived SSTs are 1.3°C and 3.2°C lower than those reconstructed from the PREGAM calcite and whole-shell measurements, respectively, but this difference is not statistically significant (see overlapping whiskers in Figure 4c).

The $\delta^{18}O_{sw}$ values reconstructed from whole-shell and GAM measurements of the core-top shells overestimate the observed value (0.33‰, VSMOW; Schmidt et al., 1999) by 1.3‰ and 0.6‰, respectively, while the average PREGAM-derived $\delta^{18}O_{sw}$ value is within 0.1‰ of the observed value (Figure 4d). The elevated $\delta^{18}O_{sw}$ values reconstructed from whole-shell and GAM measurements are primarily due to the high $\delta^{18}O$ values of the GAM calcite (Figure 4a; see section 4.2). In summation, results from the Site 806 core-top sample indicate that in situ PREGAM $\delta^{18}O$ and Mg/Ca measurements provide more accurate $\delta^{18}O_{sw}$ values than conventional whole-shell analyses with the latter consistently overestimating the observed $\delta^{18}O_{sw}$ value. Such results motivate the use of PREGAM $\delta^{18}O$ ratios to reconstruct Pliocene $\delta^{18}O_{sw}$ values.

3.3. Site 806 $\delta^{18}O$ and Mg/Ca Records (Pliocene to Early Pleistocene)

The Pliocene to earliest Pleistocene (5.1–2.2 Ma) time series of SIMS $\delta^{18}O$ data reveals that the magnitude of the PREGAM-GAM $\delta^{18}O$ offset varies through the Site 806 study section (Figure 5a). The GAM $\delta^{18}O$ values remain relatively invariant and are centered on −1.2 ± 0.1‰ VPDB (±2 SE), so variation in the PREGAM-GAM $\delta^{18}O$ offset is chiefly due to transient increases in the PREGAM $\delta^{18}O$ values. These transient increases result in the convergence of PREGAM and GAM $\delta^{18}O$ values in four samples (3.55, 3.71, 4.38, and 4.98 Ma), but three of these four samples are represented by PREGAM $\delta^{18}O$ data from only a single *T. sacculifer* shell (Figure 5a). The paucity of PREGAM $\delta^{18}O$ data for these particular samples is due to poor preservation as many of the *T. sacculifer* shells have suffered substantial degrees of internal dissolution (Figure 3). The limited PREGAM $\delta^{18}O$ data for these samples raise the likelihood that, to some degree, the transient PREGAM-GAM $\delta^{18}O$ convergences may be statistical aberrations related to under-sampling.

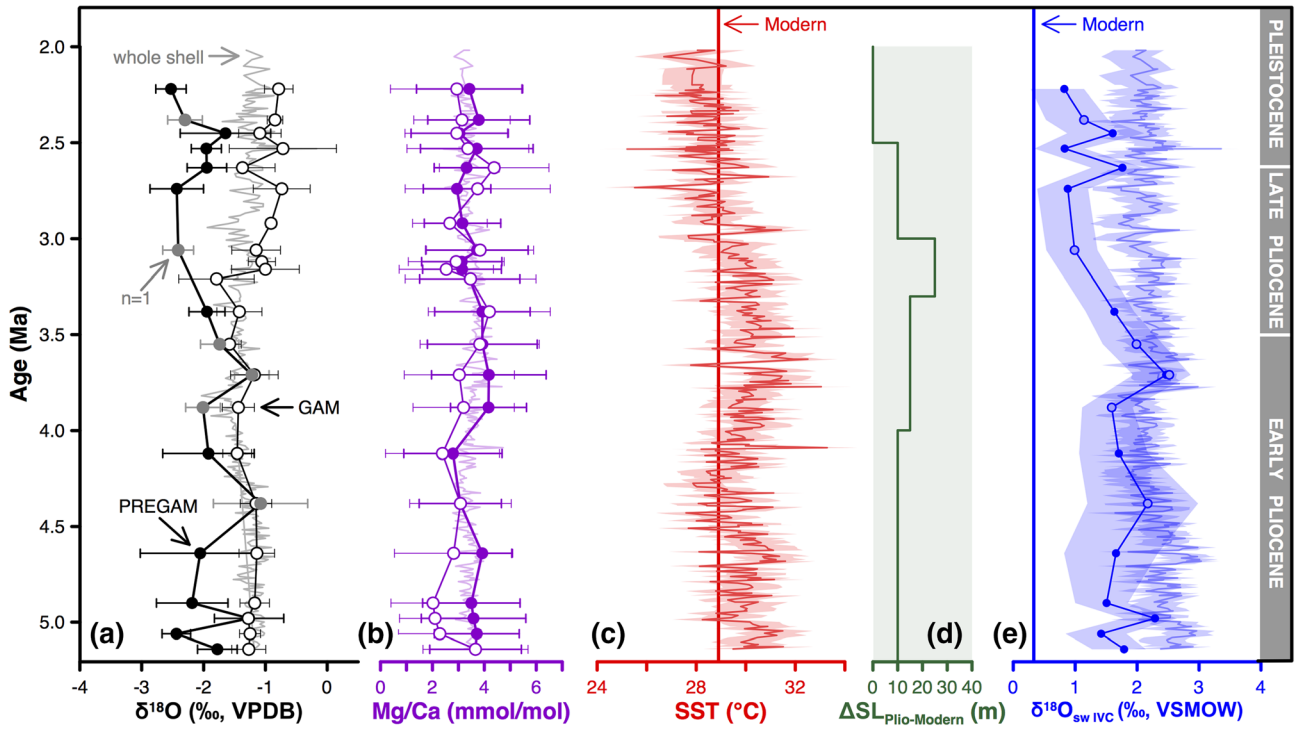

Figure 5. Plio-Pleistocene $\delta^{18}O$, Mg/Ca, SST, and IVC $\delta^{18}O_{sw}$ records for Site 806 derived from in situ (this study) and whole-shell measurements (Wara et al., 2005). (a) Time series of $\delta^{18}O$ values measured from PREGAM calcite (filled circles), GAM calcite (open circles), and whole shells (gray line). Error bars = ±2 SE. Gray circles indicate samples with PREGAM $\delta^{18}O$ from 1 shell (error bars = analytical precision, ±2 SD). (b) Time series of Mg/Ca ratios measured from PREGAM calcite (filled circles), GAM calcite (open circles), and whole shells (light purple line). Error bars = ±2 SE. (c) Calculated SSTs using Mg/Ca ratios from whole-shell measurements. Red shading = ±1.2°C (Anand et al., 2003; Dekens et al., 2002; Lea et al., 1999). (d) Pliocene-modern sea level difference ($\Delta SeaLevel_{Plio\text{-}Modern}$). Light green shading denotes range of $\Delta SeaLevel_{Plio\text{-}Modern}$ values for uncertainty on reconstructed $\delta^{18}O_{sw}$ values. (e) Ice-volume corrected (IVC) surface-ocean $\delta^{18}O_{sw}$ values for the Plio-Pleistocene study interval reconstructed from PREGAM $\delta^{18}O$ values paired with whole-shell SSTs (dark line) and whole-shell $\delta^{18}O$ values paired with whole-shell SSTs (light line). Blue shading = ± propagated error plus IVC of 0 m (maximum $\delta^{18}O_{sw}$) and 40 m (minimum $\delta^{18}O_{sw}$).

Comparison of the whole-shell and in situ $\delta^{18}O$ data for the Site 806 Pliocene section reveals that the whole-shell values are strongly skewed toward GAM values (Figure 5a). Furthermore, inter-sample variability in both the whole-shell and GAM $\delta^{18}O$ records (±0.4 and ±0.6, 2 SD, respectively) is less than that captured by the PREGAM $\delta^{18}O$ record (±0.9, 2 SD).

Unlike the $\delta^{18}O$ records, the in situ Mg/Ca ratios measured from PREGAM and GAM calcite and whole shells are similar to one another throughout the Site 806 Pliocene study section (Figure 5b). PREGAM Mg/Ca ratios (~3.8 mmol/mol) appear to be higher than those of GAM calcite (~2.1 mmol/mol) during the earliest part of the early Pliocene (5.2–4.8 Ma), but these PREGAM-GAM offsets are still within intra-sample variability. In situ Mg/Ca ratios of individual shells from a given sample are quite variable (1.9 mmol/mol, average 2 SD), but such inter-shell variability is not captured by the whole-shell Mg/Ca record because of aggregate analysis of multiple shells using conventional techniques. In short, no significant offset is detected between the in situ and whole-shell Mg/Ca ratios. Considering this result, only the SSTs reconstructed from whole-shell Mg/Ca ratios are paired with in situ and whole-shell $\delta^{18}O$ values to reconstruct $\delta^{18}O_{sw}$ values.

3.4. Pliocene SSTs at Site 806

The average PREGAM Mg/Ca ratio of each sample and its associated whole-shell Mg/Ca ratio were used to reconstruct Pliocene SSTs at Site 806 (Figure 5c). The SSTs reconstructed from whole-shell measurements track a long-term cooling of only ~1°C from 29.9°C in the early Pliocene to modern-like SSTs ~29°C by the late Pliocene (~3.0 Ma). The reconstruction indicates the WPWP was warmest during the early Pliocene with brief SST spikes up to 33.3°C and 32.5°C at 4.2 and 3.6 Ma, respectively.

3.5. Secular Variation in Pliocene Surface-Ocean $\delta^{18}O_{sw}$ at Site 806

Prior to ~3.7 Ma, the ice-volume corrected (IVC) whole-shell and PREGAM $\delta^{18}O_{sw}$ records are similar to one another ($\delta^{18}O_{sw}$ averages = 2.3‰ and 1.8‰, VSMOW, respectively) and 1.5–2.0‰ higher than the modern value (Figure 5e). The $\delta^{18}O_{sw}$ values derived from PREGAM $\delta^{18}O$ measurements decrease over the course of the late Pliocene by 1.6‰ on a slow approach toward the modern value. A similar late Pliocene-to-early Pleistocene decrease toward the modern value is not expressed in the ice-volume corrected $\delta^{18}O_{sw}$ record derived from whole-shell $\delta^{18}O$ measurements (Figure 5e).

4. Discussion

4.1. Insights Into Conventional Measurement of Whole-Shell Mg/Ca Ratios

Temperatures reconstructed from foraminifer Mg/Ca ratios are susceptible to bias by post-depositional processes, and the most problematic of these is dissolution which decreases the Mg/Ca ratios of foraminifer shells by preferential removal of high-Mg domains in the PREGAM calcite (Brown & Elderfield, 1996; Johnstone et al., 2011; Lorens et al., 1977). This process provides an explanation for the similar Mg/Ca ratios of the PREGAM and GAM calcites (Figures 2f and 5b), the latter of which is naturally Mg-depleted due to calcification in colder water (Eggins et al., 2003; Rosenthal et al., 2000). The preferential dissolution of PREGAM calcite is evidenced by etched domains within the interior of *T. sacculifer* shell walls (Figure 3 and Data Set S2) and in the low intra-shell Mg/Ca variability measured in the PREGAM calcite (1.6 mmol/mol; average 2 SD of average Mg/Ca ratios per shell) relative to the high intra-shell Mg/Ca variability of unaltered *T. sacculifer* shells grown in laboratory culture (1–14 mmol/mol; Eggins et al., 2004). Although PREGAM domains of shells analyzed in this study have been partly etched, the intra-shell Mg/Ca homogeneity explains the minimal offset between whole-shell and PREGAM Mg/Ca ratios (Figure 4b) and suggests that resulting SSTs are not the principal cause for the differences seen between the whole-shell and PREGAM $\delta^{18}O_{sw}$ records (Figure 4e).

Whole-shell Mg/Ca measurements may also be affected by the presence of early diagenetic, high-magnesium calcite coatings on foraminifer shells (Kozdon et al., 2013). The shells analyzed for this study appear frosty under optical light, which is indicative of early diagenetic alteration (Pearson et al., 2001, 2007; Sexton et al., 2006; Wycech et al., 2016). Although the presence of diagenetic calcite on the whole shells cannot be ruled out, the similarity between in situ and whole-shell records (Figure 5b) suggests that such coatings have not strongly affected the Mg/Ca ratios used in this study.

4.2. Insights Into Conventional Measurement of $\delta^{18}O_{calcite}$

The water-depth migration undertaken by *T. sacculifer* during the reproductive (gametogenesis) stage at the end of its life cycle produces significant (0.6–0.8‰) intra-shell $\delta^{18}O$ variability that masks the true surface-ocean signal in conventional $\delta^{18}O_{sw}$ records (Figure 5e; Wycech, 2017). Modern $\delta^{18}O_{sw}$ values are invariant through the upper 200 m of the water column at Site 806 (0.3 ± 0.1‰, VSMOW; Figure S3). We argue that the $\delta^{18}O_{sw}$ profile would have been similar during the Pliocene, and thus, the intra-shell $\delta^{18}O$ variability we measure is primarily due to calcification at different temperatures. Our results indicate that whole-shell $\delta^{18}O_{calcite}$ values of planktic foraminifer species that undergo an ontogenetic depth migration should not be used for interpretations of paleoceanographic conditions at a specific depth. This issue is even pervasive among *T. sacculifer* without sac-like final chambers, such as those analyzed by Wara et al. (2005). The whole-shell $\delta^{18}O_{calcite}$ values and derived reconstructions for such species predictably reflect a mixed signal that has been integrated over multiple water depths (e.g., Lohmann, 1995).

Neither the $\delta^{18}O_{calcite}$ values nor the temporal $\delta^{18}O_{calcite}$ shifts derived from conventional measurements of *T. sacculifer* should be regarded with a high degree of confidence because whole shells have variable PREGAM-GAM $\delta^{18}O_{calcite}$ differences as well as variable proportions of GAM and diagenetic calcites (e.g., Rosenthal et al., 2000; Wycech, Kelly, Kitajima, et al., 2018). For example, it is difficult to determine if minor temporal $\delta^{18}O_{calcite}$ shifts, like the ~0.4‰ oscillations in the whole-shell $\delta^{18}O_{calcite}$ record (Figure 5a), reflect a change in seawater conditions (temperature or $\delta^{18}O_{sw}$) or varying proportions of high-$\delta^{18}O$ GAM calcite among shells due to changes in preservation or GAM thickness. The importance of in situ measurements is highlighted by the fact that the PREGAM-derived $\delta^{18}O_{sw}$ values decrease

from the early to late Pliocene in the WPWP, while such a trend is not apparent in the whole-shell $\delta^{18}O_{sw}$ record (Figure 5e). We attribute this marked difference between PREGAM and whole-shell $\delta^{18}O_{sw}$ records to preferential dissolution of PREGAM calcite, which increases the proportion of high-$\delta^{18}O$ GAM and diagenetic calcites on whole shells. This is apparent in previous studies that reported a positive correlation between *T. sacculifer* $\delta^{18}O$ values and core/water depth due to partial shell dissolution (e.g., Duplessy et al., 1981; Wu & Berger, 1989). Our observation of the poor preservation of *T. sacculifer* shells at Site 806 (Figure 3) serves as a cautionary tale for paleoceanographic reconstructions performed with conventional techniques because preferential dissolution of PREGAM increases the proportion of high-$\delta^{18}O$ GAM and diagenetic calcites in whole shells (e.g., Wycech, Kelly, Kitajima, et al., 2018).

The similarity between whole-shell and GAM $\delta^{18}O$ values suggests that the shells are mostly or, in some instances, completely composed of GAM calcite (Figures 4a and 5a). The more extreme case (i.e., complete dissolution of all PREGAM calcite) seems unlikely given the visible and measurable amounts of PREGAM calcite in most shells (Figures 2c, 2d, and 3 and Data Set S2) and previous estimates of the proportion of GAM calcite on *T. sacculifer* shells (25–65%) (Bé, 1980; Caron et al., 1990; Erez & Honjo, 1981; Lohmann, 1995; Wycech, Kelly, Kitajima, et al., 2018). An added complication to this whole-shell versus in situ $\delta^{18}O$ comparison is that the conventional technique analyzes all chambers, while in situ measurements were made on only the penultimate chamber. This difference between the two analytical techniques is noteworthy because GAM calcite is thickest on the juvenile chambers (Data Set S2). Thus, whole-shell measurements may capture more of the GAM $\delta^{18}O$ value due to the aggregate analysis of all of the chambers in *T. sacculifer* shells.

Another plausible explanation for the similarity between whole-shell and GAM $\delta^{18}O$ values is measurement of high-$\delta^{18}O$ diagenetic calcite by conventional gas-source mass spectrometry requiring acid digestion of whole shells (Crowley & Zachos, 2000). This alternative explanation warrants consideration because diagenetic calcite is known to precipitate within millimeters of the sediment-water interface (Broecker, 2003; Jahnke & Jahnke, 2004) and affects the geochemistry of relatively young (Quaternary) planktic foraminifer shells (Wycech et al., 2016). Hence, the opaque ("frosty") Pliocene-aged shells analyzed in this study have likely experienced some degree of post-depositional alteration as they were recovered from sediments buried >50 m below the sea floor (e.g., Schrag et al., 1995).

The aforementioned explanations for the similar whole-shell and GAM $\delta^{18}O$ values need not be mutually exclusive. Determining whether the overlapping $\delta^{18}O$ values in these two records are due to aggregate analysis of all chambers by conventional gas-source mass spectrometry is not possible with the data at hand. We therefore turn our attention to the possible role of diagenesis. To this end, we estimate the proportion of diagenetic calcite on the whole shells by mass balance using a diagenetic $\delta^{18}O$ endmember ($\delta^{18}O_{Diagenetic}$), the unaltered whole-shell $\delta^{18}O$ endmember calculated from SIMS measurements for each sample ($\delta^{18}O_{Unaltered}$), and the measured whole-shell $\delta^{18}O$ value for each sample ($\delta^{18}O_{WholeShell}$). We first predict the $\delta^{18}O$ value of unaltered whole shells using the average PREGAM and GAM $\delta^{18}O$ values for each sample,

$$\delta^{18}O_{Unaltered} = f\,\delta^{18}O_{GAM} + (1-f)\,\delta^{18}O_{PREGAM}, \quad (1)$$

where f is the proportion of GAM calcite on the unaltered whole shell. We applied the image processing technique described in Wycech, Kelly, Kitajima, et al. (2018) to estimate the proportion of GAM calcite composing the Pliocene shells (0.25–0.54, mean = 0.37; Table S4). The maximum, minimum, and average GAM proportions are used to predict the maximum, minimum, and average unaltered whole-shell $\delta^{18}O$ value for each sample (Figure 6a). The image processing technique assumes that the proportions of PREGAM and GAM calcites on the imaged chamber reflect the proportions of the whole shell and that PREGAM dissolution occurs uniformly throughout the shell. The technique does not consider the lack of GAM calcite on internal (juvenile) chambers or the presence of the aperture (i.e., the absence of shell wall). However, the penultimate chamber of *T. sacculifer* composes a large proportion of the bulk of the shell, so image processing of the cross-sectioned penultimate chamber walls provides a first-order approximation of the amount of GAM calcite in the Site 806 *T. sacculifer* specimens.

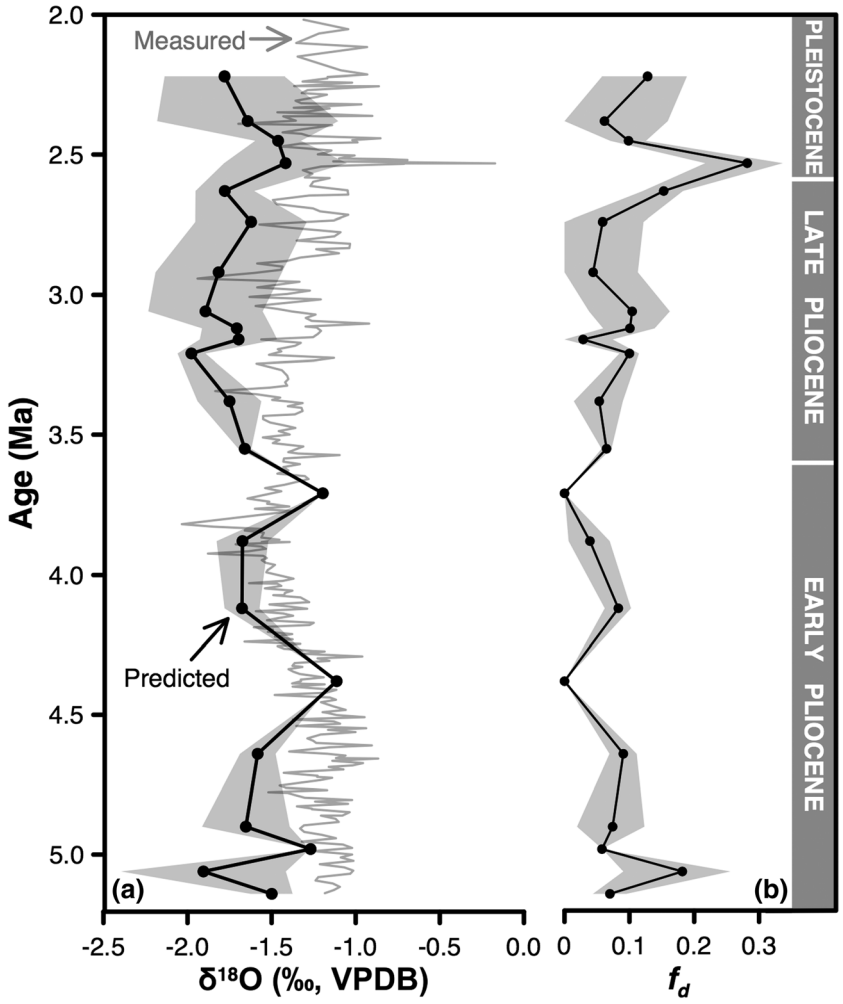

Figure 6. Estimates for diagenetic alteration of Plio-Pleistocene *Trilobatus sacculifer* shells at Site 806 (see section 4.2 for calculations). (a) Predicted whole-shell $\delta^{18}O_{calcite}$ for Site 806 (black line) calculated by PREGAM-GAM $\delta^{18}O$ mass balance plotted alongside the published (Wara et al., 2005) whole-shell $\delta^{18}O_{calcite}$ record (gray line). Shaded area = range of predicted $\delta^{18}O_{calcite}$ based on varying GAM proportions. (b) Fraction of diagenetic calcite (f_d) required to remove offsets between the predicted and published whole-shell $\delta^{18}O$ records. Lines = average f_d, shaded area = minimum and maximum f_d range based on different GAM proportions in whole shells.

The measured whole-shell $\delta^{18}O$ values can be mathematically regarded as a mass balance between the $\delta^{18}O$ of the unaltered whole shell and the $\delta^{18}O$ of diagenetic calcite,

$$\delta^{18}O_{WholeShell} = f_d\,\delta^{18}O_{Diagenetic} + (1 - f_d)\,\delta^{18}O_{Unaltered}, \quad (2)$$

where f_d is the proportion of diagenetic calcite on the measured whole shells. Rearrangement of equation (2) provides,

$$f_d = \left(\delta^{18}O_{WholeShell} - \delta^{18}O_{Unaltered}\right) / \left(\delta^{18}O_{Diagenetic} - \delta^{18}O_{Unaltered}\right). \quad (3)$$

The predicted $\delta^{18}O_{Diagenetic}$ value for Site 806 is 3.2‰ (VPDB) based on modern observed bottom water temperature (1.8°C) and $\delta^{18}O_{sw}$ (0.03‰, VSMOW) at 2,500-m water depth (NOAA/TAO; Schmidt et al., 1999). The $\delta^{18}O_{Diagenetic}$ value was calculated with the O'Neil et al. (1969) $\delta^{18}O$-temperature calibration derived from inorganic calcite experimental measurements. The f_d records indicate that diagenetic calcite

composes a small fraction of the whole shells at Site 806 (mean = 0.09 ± 0.03, 2 SE; Figure 6b). These diagenetic estimates are plausible given that f_d values greater than 0.15 should be evident in cross-section and measurable by in situ techniques.

The implications of our mass-balance calculations for diagenesis are twofold. First, our calculations suggest that diagenesis measurably increases whole-shell $\delta^{18}O$ values even though this secondary carbonate composes a small proportion of the foraminifer shell. Second, the variable down-core proportions of diagenetic calcite on whole shells (Figure 6b) indicate that the degree of alteration is not solely dependent on burial depth in young (Plio-Pleistocene) sediments. In other words, foraminifer preservation should be investigated on a sample-to-sample basis, ideally in cross-section, prior to making paleoclimate inferences from their $\delta^{18}O$ records. These findings are significant because previous studies have used only whole-shell $\delta^{18}O_{calcite}$ values to infer either paleo-temperature or salinity conditions (e.g. Billups et al., 2007; Haug et al., 2001; Keigwin, 1982; Steph et al., 2006). In short, we posit that measurement of $\delta^{18}O$-enriched diagenetic calcite by conventional gas-source mass spectrometry is likely a contributing factor to the convergence seen between the published whole-shell and in situ GAM $\delta^{18}O$ records.

4.3. Implications for the El Padre Controversy

This study indicates that Early Pliocene SSTs at Site 806 were ~1°C warmer than modern on average, which is consistent with previous studies that also accounted for the lower Mg/Ca_{sw} ratio in the Pliocene (e.g., O'Brien et al., 2014; Figure A1a). Some previously published SST records, derived from whole-shell planktic foraminifer Mg/Ca ratios and organic geochemical proxies ($U^{k'}_{37}$ and TEX_{86}), reconstruct modern-like SSTs at Site 806 during the early Pliocene (Figure A1a; Andersson, 1997; Pagani et al., 2010; Rickaby & Halloran, 2005; Wara et al., 2005; Zhang et al., 2014). However, modern-like SSTs for the early Pliocene WPWP are suspect given that these previous foraminifer Mg/Ca-derived records did not account for Pliocene Mg/Ca_{sw} ratios and the fact that $U^{k'}_{37}$ is an imprecise paleothermometer at temperatures greater than 30°C (Tierney & Tingley, 2018). These discrepancies notwithstanding, we note that the Pliocene SST record presented in this study for Site 806 (revised from Wara et al., 2005) was included in a recent statistical multi-proxy reconstruction of equatorial Pacific SSTs (Wycech et al., 2019). The study concluded that the Pliocene west-east SST difference was reduced by 4.4°C relative to the recent (0–0.5 Ma) average, which is consistent with El Padre conditions during the early Pliocene.

Contrary to numerous studies and multiple lines of evidence for persistent El Padre during the Pliocene (Molnar & Cane, 2007), earlier $\delta^{18}O_{sw}$ reconstructions from conventional whole-shell analyses of *T. sacculifer* at Site 806 argue for permanent La Niña-like conditions during the Pliocene (Rickaby & Halloran, 2005; Figure A1b). However, this whole-shell $\delta^{18}O_{sw}$ record is likely aliased due to low sampling resolution and is derived from unrealistic, cool temperatures for the WPWP (~25°C; Figure A1a). Our study reconstructs early Pliocene WPWP $\delta^{18}O_{sw}$ values (~1.8‰ VSMOW ice-volume corrected) that are significantly higher than modern values (0.3‰ VSMOW) in this region (Figures 5e and A1b). This finding indicates that the western equatorial Pacific was more arid (drier) than today, which is consistent with strong ("super") El Niño events during which the western fresh pool shifts eastward and detaches from the warm pool (Zhao et al., 2016). The termination of an El Padre state and the strengthening of Walker Circulation is signaled by the shift toward modern-like, in situ-derived $\delta^{18}O_{sw}$ values around 3.5 Ma (Figure 5e). Furthermore, the late Pliocene $\delta^{18}O_{sw}$ shift in the Site 806 in situ record is coincident with oceanographic changes in the eastern equatorial Pacific (i.e., shoaling of the thermocline and sea-surface cooling), which in combination with our Site 806 $\delta^{18}O_{sw}$ record, corroborate the view that El Padre ceased during the late Pliocene (Cannariato & Ravelo, 1997; Chaisson & Ravelo, 2000; Steph et al., 2010; X. Zhang et al., 2012). We therefore attribute the late Pliocene decrease in WPWP $\delta^{18}O_{sw}$ values to the closure of the Central American Seaway and gradual constriction of the Indonesian Seaway—tectonic events that undoubtedly impacted atmospheric and ocean circulation patterns (e.g., Cane & Molnar, 2001; Cannariato & Ravelo, 1997; Chaisson & Ravelo, 2000; Gourlan et al., 2008; Haug et al., 2001; Rai & Singh, 2012).

Unlike the PREGAM-derived $\delta^{18}O_{sw}$ record, the Site 806 whole-shell-derived $\delta^{18}O_{sw}$ record does not capture the termination of El Padre in the late Pliocene (Figure 5e). We attribute this discrepancy to the erroneously

high whole-shell $\delta^{18}O_{calcite}$ values caused by the combined effects of PREGAM calcite dissolution with attendant increases in the proportions of $\delta^{18}O$-enriched GAM and/or diagenetic calcite on the whole shells. Although whole-shell-derived $\delta^{18}O_{sw}$ values are estimated to have high uncertainty (~0.6‰, 1σ; Rohling, 2000; Schmidt, 1999), the ~2‰ difference between PREGAM and whole-shell $\delta^{18}O_{sw}$ values during the early Pleistocene is still significant (Figure 5e). This finding highlights how in situ analyses improve the accuracy of paleo-$\delta^{18}O_{sw}$ records derived from *T. sacculifer* shells through the targeting of only PREGAM calcite, which eliminates high-$\delta^{18}O$ signals of GAM and diagenetic calcites on whole shells. Measurements from the core-top sample at Site 806 corroborate our assertion for improved accuracy in the in situ-derived $\delta^{18}O_{sw}$ reconstruction (Figure 4d). For this reason, we consider the early to late Pliocene decrease in PREGAM-derived $\delta^{18}O_{sw}$ values to be a robust signal of progressive freshening in the WPWP and termination of El Padre.

5. Conclusions

In situ measurements carried out on micrometer-scale domains within individual fossil shells of the planktic foraminifer *T. sacculifer* from the western equatorial Pacific (ODP Site 806) show that the $\delta^{18}O$ value of GAM calcite is ~0.6–0.8‰ higher than that of PREGAM calcite, while the Mg/Ca ratios of the GAM and PREGAM calcites are statistically indistinguishable. We therefore conclude that published whole-shell $\delta^{18}O_{calcite}$ values for the Pliocene WPWP (Wara et al., 2005) are biased toward the high-$\delta^{18}O$ GAM endmember especially when the PREGAM calcite is dissolved and high-$\delta^{18}O$ diagenetic calcite is added to the shells. The shells analyzed from Site 806 were frosty in appearance, and a mass-balance model of whole-shell and in situ $\delta^{18}O$ values indicates that diagenetic calcite may compose up to 28% of some *T. sacculifer* shells. The degree of diagenesis varies in our Pliocene study samples, but the presence of GAM crust on the majority of analyzed *T. sacculifer* shells consistently introduces inaccuracies to whole-shell $\delta^{18}O_{calcite}$ measurements and the $\delta^{18}O_{sw}$ values derived from them.

After adjusting for a lower Mg/Ca ratio of Pliocene seawater, the SST record derived from published whole-shell Mg/Ca ratios (Wara et al., 2005) indicates that the early Pliocene WPWP was, on average, ~1°C warmer than today and cooled to the modern SST in the late Pliocene (Figure 5c). The ice-volume corrected $\delta^{18}O_{sw}$ values reconstructed from paired $\delta^{18}O$ and Mg/Ca ratios of whole shells and PREGAM calcite are ~2‰ higher than the modern value in the early Pliocene (Figure 5e), indicating that surface waters at Site 806 were more saline relative to modern. This suggests that a more arid climatic regime prevailed in the WPWP during the early Pliocene, which is consistent with the El Padre state posited to have existed at that time (e.g., Ravelo et al., 2014; Wara et al., 2005). However, congruency between the two parallel $\delta^{18}O_{sw}$ records breaks down during the late Pliocene as PREGAM-derived $\delta^{18}O_{sw}$ values begin to decrease toward the modern WPWP $\delta^{18}O_{sw}$ value while whole-shell $\delta^{18}O_{sw}$ values remain ~2‰ higher than modern (Figure 5e). We attribute the divergence between the two $\delta^{18}O_{sw}$ records to enhanced dissolution of PREGAM calcite, which increases the proportion of high-$\delta^{18}O$ GAM and/or diagenetic calcite on the whole shells recovered from the late Pliocene section of Site 806.

Establishment of modern Walker circulation, signaled by the decrease in WPWP $\delta^{18}O_{sw}$ values derived from PREGAM measurements at ~3.7 Ma, is coincident with paleoceanographic changes in the Indian Ocean and eastern equatorial Pacific that have been attributed to the combined effects of gradual constriction of the Indonesian Seaway and closure of the Central American Seaway (Cane & Molnar, 2001; Cannariato & Ravelo, 1997; Haug et al., 2001; Rai & Singh, 2012). Our records of Pliocene WPWP hydroclimate motivate further investigation into whether El Padre conditions prevailed during what many climate scientists consider to be an informative analog for ongoing and future climate change.

Appendix A: Summary of Previously Published SSTs and $\delta^{18}O_{sw}$ Values

The SSTs and $\delta^{18}O_{sw}$ values previously reported are compared to the in situ SSTs and $\delta^{18}O_{sw}$ values reconstructed in this study. All records depicted in Figure A1 are as they are reported in the respective publication.

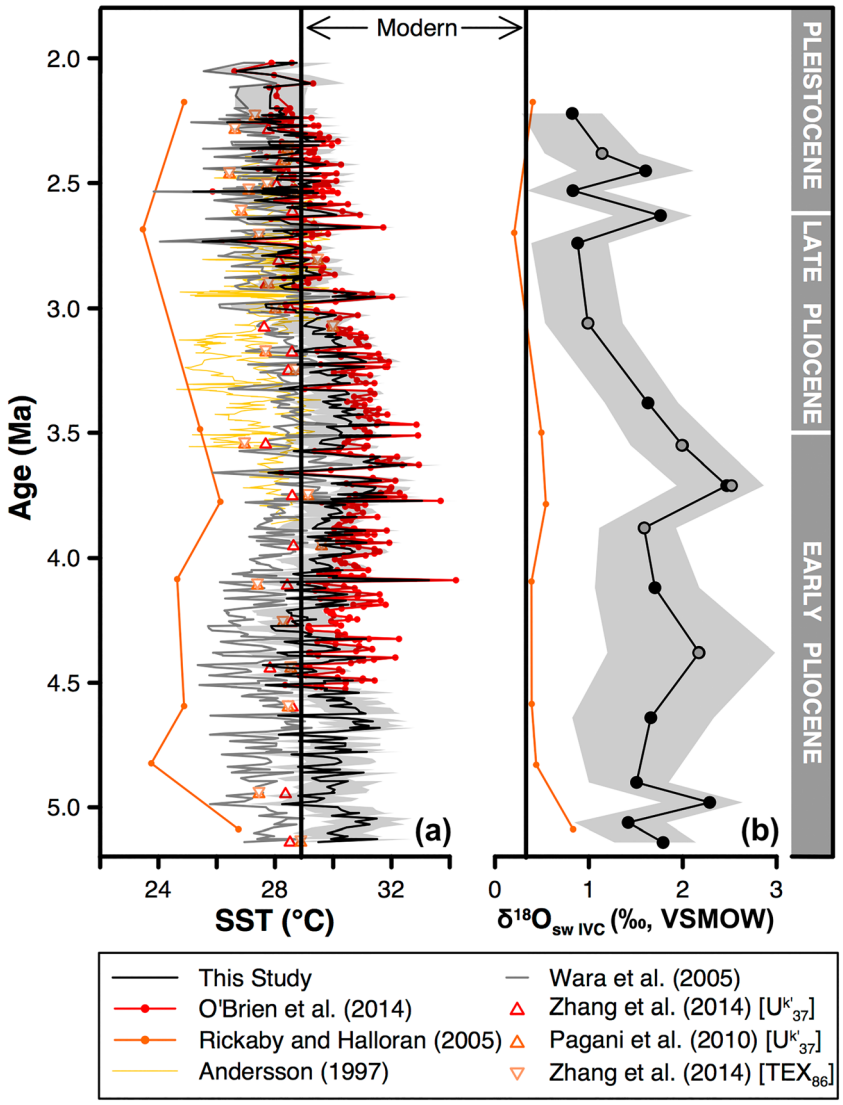

Figure A1. Previously published SST and $\delta^{18}O_{sw}$ records for the Site 806 Plio-Pleistocene study interval. (a) SSTs derived from whole-shell Mg/Ca ratios of *Trilobatus sacculifer* (O'Brien et al., 2014; Rickaby & Halloran, 2005; Wara et al., 2005), planktic foraminifer assemblages (Andersson, 1997), and organic proxies (Pagani et al., 2010; Zhang et al., 2014). SSTs recalculated from Wara et al., 2005 (this study). Dark gray shading = ±1.2°C (Anand et al., 2003; Dekens et al., 2002; Lea et al., 1999). (b) Ice-volume corrected (IVC) $\delta^{18}O_{sw}$ values from paired $\delta^{18}O$:Mg/Ca ratios of whole shells (Rickaby & Halloran, 2005) and PREGAM $\delta^{18}O$ values paired with whole-shell SSTs (black line and shading, this study). Gray area = ± propagated error plus IVC of 0 m (maximum $\delta^{18}O_{sw}$) and 40 m (minimum $\delta^{18}O_{sw}$).

Acknowledgments

Funding courtesy the University of Wisconsin-Madison Geoscience Department Graduate Student Summer Research Funds (2013–2016) and the Geoscience Department Twenhofel Award (Wycech). Support for this research was also provided by the University of Wisconsin-Madison Office of the Vice Chancellor for Research and Graduate Education with funding from the Wisconsin Alumni Research Foundation (Kelly). WiscSIMS is supported by the National Science Foundation (EAR-1355590 and EAR-1658823) and the University of Wisconsin-Madison. This research used samples provided by the Ocean Drilling Program (ODP). ODP was funded through the National Science Foundation (NSF) and participating countries under the management of Joint Oceanographic Institutions (JOI), Inc. Site 806 observed temperatures from Tropical Atmosphere Ocean (TAO) Array (GTMBA Project Office of NOAA/PMEL). Epoxy mounts were prepared by Brian Hess. SIMS measurements were assisted by Noriko Kita and John Valley. SEM imaging was assisted by Phil Gopon and Bil Schneider. Image processing was assisted by Krishna Dasari and Begum Unal (CU Science Discovery STEM Research Experience). The new data presented are also available in the National Center for Environmental Information Database (https://www.ncdc.noaa.gov/paleo/study/29632).

References

Anand, P., Elderfield, H., & Conte, M. H. (2003). Calibration of Mg/Ca thermometry in planktonic foraminifera from a sediment trap time series. *Paleoceanography*, *18*, 1–15. https://doi.org/10.1029/2002pa000846

Andersson, C. (1997). Transfer function VS modern analog technique for estimating Pliocene sea-surface temperatures based on planktic foraminiferal data, western equatorial Pacific Ocean. *Journal of Foraminiferal Research*, *27*, 123–132. https://doi.org/10.2113/gsjfr.27.2.123

Bartoli, G., Sarnthein, M., Weinelt, M., Erlenkeuser, H., Garbe-Schönberg, D., & Lea, D. W. (2005). Final closure of Panama and the onset of northern hemisphere glaciation. *Earth and Planetary Science Letters*, *237*, 33–44. https://doi.org/10.1016/j.epsl.2005.06.020

Bé, A. W. (1980). Gametogenic calcification in a spinose planktonic foraminifer, *Globigerinoides sacculifer* (Brady). *Marine Micropaleontology*, *5*, 283–310. https://doi.org/10.1016/0377-8398(80)90014-6

Bemis, B. E., Spero, H. J., Bijma, J., & Lea, D. W. (1998). Reevaluation of the oxygen isotopic composition of planktonic foraminifera: Experimental results and revised paleotemperature equations. *Paleoceanography*, *13*, 150–160. https://doi.org/10.1029/98pa00070

Bigg, G. R., & Rohling, E. J. (2000). An oxygen isotope data set for marine waters. *Journal of Geophysical Research*, *105*, 8527–8535. https://doi.org/10.1029/2000jc900005

Billups, K., Ravelo, A. C., & Zachos, J. C. (2007). Early Pliocene climate: A perspective from the western equatorial Atlantic warm pool. *Paleoceanography*, *13*, 459–470. https://doi.org/10.1029/98pa02262

Bjerknes, J. (1969). Atmospheric teleconnections from the equatorial Pacific. *Monthly Weather Review*, *97*, 163–172. https://doi.org/10.1175/1520-0493(1969)097<0163:atftep>2.3.co;2

Broecker, W. S. (2003). Does the trigger for abrupt climate change reside in the ocean or in the atmosphere? *Science*, *300*(5625), 1519–1522. https://doi.org/10.1126/science.1083797

Brown, S. J., & Elderfield, H. (1996). Variations in Mg/Ca and Sr/Ca ratios of planktonic foraminifera caused by postdepositional dissolution: Evidence of shallow Mg-dependent dissolution. *Paleoceanography*, *11*, 543–551. https://doi.org/10.1029/96pa01491

Cane, M. A., & Molnar, P. (2001). Closing of the Indonesian seaway as a precursor to east African aridification around 3-4 million years ago. *Nature*, *411*(6834), 157–162. https://doi.org/10.1038/35075500

Cannariato, K. G., & Ravelo, A. C. (1997). Pliocene-Pleistocene evolution of eastern tropical surface water circulation and thermocline depth. *Paleoceanography*, *12*, 805–820. https://doi.org/10.1029/97pa02514

Caron, D. A., Anderson, O. R., Lindsey, J. L., Faber, W. W. Jr., & Lim, E. L. (1990). Effects of gametogenesis on test structure and dissolution of some spinose planktonic foraminifera and implications for test preservation. *Marine Micropaleontology*, *16*, 93–116. https://doi.org/10.1016/0377-8398(90)90031-G

Chaisson, W. P., & Ravelo, A. C. (2000). Pliocene development of the east-west hydrographic gradient in the equatorial Pacific. *Paleoceanography*, *15*, 497–505. https://doi.org/10.1029/1999pa000442

Crowley, T. (1996). Pliocene climates: The nature of the problem. *Marine Micropaleontology*, *27*, 3–12. https://doi.org/10.1016/0377-8398(95)00049-6

Crowley, T., & Zachos, J. C. (2000). Comparison of zonal temperature profiles for past warm time periods. In B. T. Huber, K. G. MacLeod, & S. L. Wing (Eds.), *Warm climates in Earth history*, (pp. 50–76). Cambridge: Cambridge University Press.

Dekens, P. S., Lea, D. W., Pak, D. K., & Spero, H. J. (2002). Core top calibration of Mg/Ca in tropical foraminifera: Refining paleotemperature estimation. *Geochemistry, Geophysics, Geosystems*, *3*, 1–29. https://doi.org/10.1029/2001GC000200

Dekens, P. S., Ravelo, A. C., Mccarthy, M. D., & Edwards, C. A. (2008). A 5 million year comparison of Mg/Ca and alkenone paleothermometers. *Geochemistry, Geophysics, Geosystems*, *9*, 1–18. https://doi.org/10.1029/2007gc001931

Dowsett, H., Barron, J., & Poore, R. (1996). Middle Pliocene sea surface temperatures: A global reconstruction. *Marine Micropaleontology*, *27*, 13–25. https://doi.org/10.1016/0377-8398(95)00050-x

Dowsett, H. J., & Robinson, M. M. (2009). Mid-Pliocene equatorial Pacific sea surface temperature reconstruction: A multi-proxy perspective. *Philosophical Transactions of the Royal Society A: Mathematical, Physical and Engineering Sciences*, *367*, 109–125. https://doi.org/10.1098/rsta.2008.0206

Duplessy, J. C., Blanc, P. L., & Bé, A. W. (1981). Oxygen-18 enrichment of planktonic foraminifera due to gametogenic calcification below the euphotic zone. *Science*, *213*, 1247–1250. https://doi.org/10.1126/science.213.4513.1247

Dwyer, G. S., & Chandler, M. A. (2009). Mid-Pliocene sea level and continental ice volume based on coupled benthic Mg/Ca palaeotemperatures and oxygen isotopes. *Philosophical Transactions of the Royal Society A: Mathematical, Physical and Engineering Sciences*, *367*, 157–168. https://doi.org/10.1126/science.1140469

Eggins, S., De Deckker, P., & Marshall, J. (2003). Mg/Ca variation in planktonic foraminifera tests: Implications for reconstructing palaeo-seawater temperature and habitat migration. *Earth and Planetary Science Letters*, *212*, 291–306. https://doi.org/10.1016/S0012-821X(03)00283-8

Eggins, S., Sadekov, A., & De Deckker, P. (2004). Modulation and daily banding of Mg/Ca in tests by symbiont photosynthesis and respiration: A complication for seawater thermometry? *Earth and Planetary Science Letters*, *225*, 411–419. https://doi.org/10.1016/j.epsl.2004.06.019

Elderfield, H., & Ganssen, G. (2000). Past temperature and $\delta^{18}O$ of surface ocean waters inferred from foraminiferal Mg/Ca ratios. *Nature*, *405*, 442–445. https://doi.org/10.1038/35013033

Erez, J., & Honjo, S. (1981). Comparison of isotopic composition of planktonic foraminifer in plankton tows, sediment traps, and sediments. *Palaeogeography, Palaeoclimatology, Palaeoecology*, *33*, 129–156. https://doi.org/10.1016/0031-0182(81)90035-3

Erez, J., & Luz, B. (1983). Experimental paleotemperature equation for planktonic foraminifera. *Geochimica et Cosmochimica Acta*, *47*, 1025–1031. https://doi.org/10.1016/0016-7037(83)90232-6

Fehrenbacher, J., & Martin, P. (2010). Mg/Ca variability of the planktonic foraminifera *G. ruber s.s.* and *N. dutertrei* from shallow and deep cores determined by electron microprobe image mapping. *IOP Conference Series: Earth and Environmental Science*, *9*, 1–7. https://doi.org/10.1088/1755-1315/9/1/012018

Fehrenbacher, J. S., & Martin, P. (2014). Exploring the dissolution effect on the intrashell Mg/Ca variability of the planktic foraminifer *Globigerinoides ruber*. *Paleoceanography*, *29*, 854–868. https://doi.org/10.1002/2013PA002571

Ford, H. L., Ravelo, A. C., Dekens, P. S., LaRiviere, J. P., & Wara, M. W. (2015). The evolution of the equatorial thermocline and the early Pliocene El Padre mean state. *Geophysical Research Letters*, *42*, 4878–4887. https://doi.org/10.1002/2015gl064215

Ford, H. L., Ravelo, A. C., & Hovan, S. (2012). A deep eastern equatorial Pacific thermocline during the early Pliocene warm period. *Earth and Planetary Science Letters*, *355-356*, 152–161. https://doi.org/10.1016/j.epsl.2012.08.027

Gourlan, A. T., Meynadier, L., & Allègre, C. J. (2008). Tectonically driven changes in the Indian Ocean circulation over the last 25 Ma: Neodymium isotope evidence. *Earth and Planetary Science Letters*, *267*, 353–364. https://doi.org/10.1016/j.epsl.2007.11.054

Groeneveld, J. (2005). *Effect of the Pliocene closure of the Panamanian Gateway on Caribbean and east Pacific sea surface temperatures and salinities by applying combined Mg/Ca and $\delta^{18}O$ measurements (5.6–2.2 Ma) (Doctoral Dissertation)*. Retrieved from GEOMAR Repository. (http://oceanrep.geomar.de/207). Kiel, Germany: Christian-Albrechts-Universität Kiel.

Groeneveld, J., Hathorne, E. C., Steinke, S., DeBey, H., Mackensen, A., & Tiedemann, R. (2014). Glacial induced closure of the Panamanian Gateway during Marine Isotope Stages (MIS) 95–100 (+2.5 Ma). *Earth and Planetary Science Letters*, *404*, 296–306. https://doi.org/10.1016/j.epsl.2014.08.007

Groeneveld, J., Nürnberg, D., Tiedemann, R., Reichart, G. J., Steph, S., Reuning, L., et al. (2008). Foraminiferal Mg/Ca increase in the Caribbean during the Pliocene: Western Atlantic Warm Pool formation, salinity influence, or diagenetic overprint? *Geochemistry, Geophysics, Geosystems*, *9*, 1–21. https://doi.org/10.1029/2006GC001564

Haug, G. H., Tiedemann, R., Zahn, R. I., & Ravelo, A. C. (2001). Role of Panama uplift on oceanic freshwater balance. *Geology*, *29*, 207–210. https://doi.org/10.1130/0091-7613(2001)029<0207:ropuoo>2.0.co;2

Jahnke, R. A., & Jahnke, D. B. (2004). Calcium carbonate dissolution in deep sea sediments: Reconciling microelectrode, pore water and benthic flux chamber results. *Geochimica et Cosmochimica Acta*, *68*, 47–59. https://doi.org/10.1016/S0016-7037(03)00260-6

Jansen, E., Mayer, L. A., Backman, J., Leckie, R. M., & Takayana, T. (1993). Evolution of Pliocene climate cyclicity at Hole 806B (5–2Ma): Oxygen isotope record. In W. H. Berger, L. W. Kroenke, & L. A. Mayer (Eds.), *Proceedings of the Ocean Drilling Program scientific results* (Vol. 130, pp. 349–362). College Station, TX: Ocean Drilling Program.

Johnstone, H. J. H., Yu, J., Elderfield, H., & Schulz, M. (2011). Improving temperature estimates derived from Mg/Ca of planktonic foraminifera using X-ray computed tomography–based dissolution index, XDX. *Paleoceanography*, *26*, 1–17. https://doi.org/10.1029/2009PA001902

Keigwin, L. (1982). Isotopic paleoceanography of the Caribbean and East Pacific: Role of Panama uplift in late Neogene time. *Science*, *217*(4557), 350–353. https://doi.org/10.1126/science.217.4557.350

Killingley, J. S. (1983). Effects of diagenetic recrystallization on $^{18}O/^{16}O$ values of deep-sea sediments. *Nature*, *301*, 594–597. https://doi.org/10.1038/301594a0

Kita, N. T., Ushikubo, T., Fu, B., & Valley, J. W. (2009). High precision SIMS oxygen isotope analysis and the effect of sample topography. *Chemical Geology*, *264*, 43–57. https://doi.org/10.1016/j.chemgeo.2009.02.012

Kozdon, R., Kelly, D. C., Kitajima, K., Strickland, A., Fournelle, J. H., & Valley, J. W. (2013). *In situ* $\delta^{18}O$ and Mg/Ca analyses of diagenetic and planktic foraminiferal calcite preserved in a deep-sea record of the Paleocene-Eocene thermal maximum. *Paleoceanography*, *28*, 517–528. https://doi.org/10.1002/palo.20048

Kozdon, R., Ushikubo, T., Kita, N. T., Spicuzza, M. J., & Valley, J. W. (2009). Intratest oxygen isotope variability in the planktonic foraminifer *N. pachyderma*: Real vs. apparent vital effects by ion microprobe. *Chemical Geology*, *258*, 327–337. https://doi.org/10.1016/j.chemgeo.2008.10.032

Krantz, D. E. (1991). A chronology of Pliocene sea-level fluctuations: The U.S. Middle Atlantic Coastal Plain record. *Quaternary Science Reviews*, *10*, 163–174. https://doi.org/10.1016/0277-3791(91)90016-n

Krishna-Kumar, K., Rajagopalan, B., Hoerling, M., Bates, G., & Cane, M. (2006). Unraveling the mystery of Indian monsoon failure during El Niño. *Science*, *314*, 113–115. https://doi.org/10.1126/science.1131914

Lawrence, K. T., Liu, Z., & Herbert, T. D. (2006). Evolution of the eastern tropical Pacific through Plio-Pleistocene glaciation. *Science*, *312*(5770), 79–83. https://doi.org/10.1126/science.1120395

Lea, D. W., Mashiotta, T. A., & Spero, H. J. (1999). Controls on magnesium and strontium uptake in planktonic foraminifera determined by live culturing. *Geochimica et Cosmochimica Acta*, *63*, 2369–2379. https://doi.org/10.1016/S0016-7037(99)00197-0

Lipps, J. H., & Ribbe, P. H. (1967). Electron-probe microanalysis of planktonic foraminifera. *Journal of Paleontology*, *41*, 492–496. Retrieved from https://www.jstor.org/stable/1302028

Locarnini, R. A.Mishonov A. V., Antonov, J. I., Boyer, T. P., Garcia, H. E., Baranova, O. K., et al. (2013). World ocean atlas 2013, volume 1: Temperature. In S. Levitus, & A. Mishonov (Eds.), *NOAA atlas* (Vol. *73*, pp. 1–40). Silver Spring, MD: NESDIS.

Lohmann, G. P. (1995). A model for variation in the chemistry of planktonic foraminifera due to secondary calcification and selective dissolution. *Paleoceanography*, *10*, 445–457. https://doi.org/10.1029/95pa00059

Lorens, R. B., Williams, D. F., & Bender, M. (1977). The early nonstructural chemical diagenesis of foraminiferal calcite. *Journal of Sedimentary Petrology*, *47*, 1602–1609. https://doi.org/10.1306/212F73C9-2B24-11D7-8648000102C1865D

Medina-Elizalde, M., Lea, D. W., & Fantle, M. S. (2008). Implications of seawater Mg/Ca variability for Plio-Pleistocene tropical climate reconstruction. *Earth and Planetary Science Letters*, *269*, 585–595. https://doi.org/10.1016/j.epsl.2008.03.014

Miller, K. G., Fairbanks, R. G., & Mountain, G. S. (1987). Tertiary oxygen isotope synthesis, sea level history, and continental margin erosion. *Paleoceanography*, *2*, 1–19. https://doi.org/10.1029/pa002i001p00001

Molnar, P., & Cane, M. A. (2002). El Niño's tropical climate and teleconnections as a blueprint for pre-Ice Age climates. *Paleoceanography*, *17*, 1–13. https://doi.org/10.1029/2001pa000663

Molnar, P., & Cane, M. A. (2007). Early Pliocene (pre–Ice Age) El Niño–like global climate: Which El Niño? *Geosphere*, *3*, 337–365. https://doi.org/10.1130/GES00103.1

Mulitza, S., Boltovskoy, D., Donner, B., Meggers, H., Paul, A., & Wefer, G. (2003). Temperature:$\delta^{18}O$ relationships of planktonic foraminifera collected from surface waters. *Palaeogeography, Palaeoclimatology, Palaeoecology*, *202*, 143–152. https://doi.org/10.1016/S0031-0182(03)00633-3

Nürnberg, D., Bijma, J., & Hemleben, C. (1996). Assessing the reliability of magnesium in foraminiferal calcite as a proxy for water mass temperatures. *Geochimica et Cosmochimica Acta*, *60*, 803–814. https://doi.org/10.1016/0016-7037(95)00446-7

O'Brien, C. L., Foster, G. L., Martínez-Botí, M. A., Abell, R., Rae, J. W. B., & Pancost, R. D. (2014). High sea surface temperatures in tropical warm pools during the Pliocene. *Nature Geoscience*, *7*, 606–611. https://doi.org/10.1038/NGEO2194

O'Neil, J. R., Clayton, R. N., & Mayeda, T. K. (1969). Oxygen isotope fractionation in divalent metal carbonates. *The Journal of Chemical Physics*, *51*, 5547–5558. https://doi.org/10.1063/1.1671982

Pagani, M., Liu, Z., Lariviere, J., & Ravelo, A. C. (2010). High Earth-system climate sensitivity determined from Pliocene carbon dioxide concentrations. *Nature Geoscience*, *3*, 27–30. https://doi.org/10.1038/ngeo724

Kroenke, L. W., Janecek, T. R., Backman, J., Bassinot, F., Corfield, R. M., Delaney, M. L., et al. , & (1991). Site 806. In W. L. Kroenke, W. H. Berger, T. R. Janecek, et al. (Eds.), *Proceedings of the Ocean Drilling Program, initial reports* (Vol. *130*, pp. 291–267). College Station, TX: Ocean Drilling Program.

Pearson, P. N., Ditcheld, P. W., Singano, J., Harcourt-Brown, K. G., Nicholas, C. J., Shackleton, N. J., & Hall, M. A. (2001). Warm tropical sea surface temperatures in the Late Cretaceous and Eocene epochs. *Nature*, *415*, 481–487. https://doi.org/10.1038/35097000

Pearson, P. N., Van Dongen, B. E., Nicholas, C. J., Pancost, R. D., Schouten, S., Singano, J. M., & Wade, B. S. (2007). Stable warm tropical climate through the Eocene epoch. *Geology*, *35*, 211–214. https://doi.org/10.1130/g23175a.1

Philander, S. G., & Fedorov, A. V. (2003). Role of tropics in changing the response to Milankovich forcing some three million years ago. *Paleoceanography*, *18*, 1–11. https://doi.org/10.1029/2002pa000837

Rai, A. K., & Singh, V. B. (2012). Response of eastern Indian Ocean (ODP Site 762B) benthic foraminiferal assemblages to the closure of the Indonesian seaway. *Oceanologia*, *54*, 449–472. https://doi.org/10.5697/oc.54-3.449

Rausch, S., Bohm, F., Bach, W., Klugel, A., & Eisenhauer, A. (2012). Calcium carbonate veins in ocean crust record a threefold increase of seawater Mg/Ca in the past 30 million years. *Earth and Planetary Science Letters*, *362*(C), 215–224. https://doi.org/10.1016/j.epsl.2012.12.005

Ravelo, A. C., Dekens, P. S., & McCarthy, M. (2006). Evidence for El Niño–like conditions during the Pliocene. *GSA Today*, *16*, 4–11. https://doi.org/10.1130/1052-5173(2006)016<4:efenlc>2.0.co;2

Ravelo, A. C., Lawrence, K. T., Fedorov, A. V., & Ford, H. L. (2014). Comment on "a 12-million-year temperature history of the tropical Pacific Ocean". *Science*, *346*(6216), 1–5. https://doi.org/10.1126/science.1257618

Regenberg, M., Steph, S., Nürnberg, D., Tiedemann, R., & Garbe-Schönberg, D. (2009). Calibrating Mg/Ca ratios of multiple planktonic foraminiferal species with δ^{18}O-calcification temperatures: Paleothermometry for the upper water column. *Earth and Planetary Science Letters*, *278*, 324–336. https://doi.org/10.1016/j.epsl.2008.12.019

Rickaby, R. E. M., & Halloran, P. R. (2005). Cool La Niña during the warmth of the Pliocene? *Science*, *307*, 1948–1952. https://doi.org/10.1126/science.1104666

Rohling, E. J. (2000). Paleosalinity: Confidence limits and future applications. *Marine Geology*, *163*, 1–11. https://doi.org/10.1016/S0025-3227(99)00097-3

Ropelewski, C. F., & Halpert, M. S. (1987). Global and regional scale precipitation patterns associated with the El Niño/Southern Oscillation. *Monthly Weather Review*, *115*, 1606–1626. https://doi.org/10.1175/1520-0493(1987)115<1606:garspp>2.0.co;2

Ropelewski, C. F., & Halpert, M. S. (1996). Quantifying southern oscillation-precipitation relationships. *Journal of Climate*, *9*, 1043–1059. https://doi.org/10.1175/1520-0442(1996)009<1043:qsopr>2.0.co;2

Rosenthal, Y., Lohmann, G. P., Lohmann, K. C., & Sherrell, R. M. (2000). Incorporation and preservation of Mg in Globigerinoides sacculifer: Implications for reconstructing the temperature and 18O/16O of seawater. *Paleoceanography*, *15*, 135–145. https://doi.org/10.1029/1999pa000415

Sadekov, A., Eggins, S. M., De Deckker, P., Ninnemann, U., Kuhnt, W., & Bassinot, F. (2009). Surface and subsurface seawater temperature reconstruction using Mg/Ca microanalysis of planktonic foraminifera *Globigerinoides ruber*, *Globigerinoides sacculifer*, and *Pulleniatina obliquiloculata*. *Paleoceanography*, *24*(3), PA3201. https://doi.org/10.1029/2008pa001664

Sadekov, A. Y., Eggins, S. M., & De Deckker, P. (2005). Characterization of Mg/Ca distributions in planktonic foraminifera species by electron microprobe mapping. *Geochemistry, Geophysics, Geosystems*, *6*(12), 1–14. https://doi.org/10.1029/2005GC000973

Schiebel, R., & Hemleben, C. (2005). Modern planktic foraminifera. *Paläontologische Zeitschrift*, *79*(1), 135–148. https://doi.org/10.1007/bf03021758

Schmidt, G. A. (1999). Error analysis of paleosalinity calculations. *Paleoceanography*, *14*, 422–429. https://doi.org/10.1029/1999pa900008

Schmidt, G. A., Bigg, G. R., & Rohling, E. J. (1999). *Global sea-water oxygen-18 database*, New York City: NASA Goddard Institute for Space Studies (GISS). https://data.giss.nasa.gov/o18data/

Schrag, D. P., DePaolo, D. J., & Richter, F. M. (1995). Reconstructing past sea surface temperatures: Correcting for diagenesis of bulk marine carbonate. *Geochimica et Cosmochimica Acta*, *59*, 2265–2278. https://doi.org/10.1016/0016-7037(95)00105-9

Seki, O., Foster, G. L., Schmidt, D. N., Mackensen, A., Kawamura, K., & Pancost, R. D. (2010). Alkenone and boron-based pCO_2 records. *Earth and Planetary Science Letters*, *292*, 201–211. https://doi.org/10.1016/j.epsl.2010.01.037

Seki, O., Schmidt, D. N., Schouten, S., Hopmans, E. C., Sinninghe Damsté, J. S., & Pancost, R. D. (2012). Paleoceanographic changes in the eastern equatorial Pacific over the last 10 Myr. *Paleoceanography*, *27*, 1–14. https://doi.org/10.1029/2011pa002158

Sexton, P. F., Wilson, P. A., & Pearson, P. N. (2006). Microstructural and geochemical perspectives on planktic foraminiferal preservation: "Glassy" versus 'frosty'. *Geochemistry, Geophysics, Geosystems*, *7*, 1–29. https://doi.org/10.1029/2006gc001291

Spero, H., & Lea, D. W. (1993). Intraspecific stable isotope variability in the planktic foraminifera *Globigerinoides sacculifer*: Results from laboratory experiments. *Marine Micropaleontology*, *22*, 221–234. https://doi.org/10.1016/0377-8398(93)90045-Y

Spero, H., Mielke, K. M., Kalve, E. M., Lea, D. W., & Pak, D. K. (2003). Multispecies approach to reconstructing eastern equatorial Pacific thermocline hydrography during the past 360 kyr. *Paleoceanography*, *18*, 1–16. https://doi.org/10.1029/2002pa000814

Steph, S., Tiedemann, R., Prange, M., Groeneveld, J., Nürnberg, D., Reuning, L., et al. (2006). Changes in Caribbean surface hydrography during the Pliocene shoaling of the Central American Seaway. *Paleoceanography*, *21*, 1–25. https://doi.org/10.1029/2004pa001092

Steph, S., Tiedemann, R., Prange, M., Groeneveld, J., Schulz, M., Timmermann, A., et al. (2010). Early Pliocene increase in thermohaline overturning: A precondition for the development of the modern equatorial Pacific cold tongue. *Paleoceanography*, *25*(2), 1–17. https://doi.org/10.1029/2008pa001645

Tierney, J. E., & Tingley, M. P. (2018). BAYSPLINE: A new calibration for the alkenone paleothermometer. *Paleoceanography and Paleoclimatology*, *33*(3), 281–301. https://doi.org/10.1016/j.palaeo.2005.11.033

Valley, J. W., & Kita, N. T. (2009). In situ oxygen isotope geochemistry by ion microprobe. In M. Fayek (Ed.), *Secondary ion mass spectrometry in the earth sciences, gleaning the big picture from a small spot* (Vol. 41, pp. 16–63). Toronto: Mineralogical Association of Canada.

Wang, C. (2004). ENSO, Atlantic climate variability, and the Walker and Hadley circulations. In H. F. Diaz, & R. S. Bradley (Eds.), *The Hadley Circulation: Present, Past and Future* (pp. 173–202). Dordrecht: Springer.

Wara, M. W., Ravelo, A. C., & Delaney, M. G. L. (2005). Permanent El Niño-like conditions during the Pliocene warm period. *Science*, *309*(5735), 758–761. https://doi.org/10.1126/science.1112596

Wardlaw, B. R., & Quinn, T. M. (1991). The record of Pliocene sea-level change at Enewetak Atoll. *Quaternary Science Reviews*, *10*, 247–258. https://doi.org/10.1016/0277-3791(91)90023-n

Wu, G., & Berger, W. H. (1989). Planktonic foraminifera: Differential dissolution and the Quaternary stable isotope record in the Western Equatorial Pacific. *Paleoceanography*, *4*(2), 181–198. https://doi.org/10.1029/pa004i002p00181

Wycech, J. (2017). *Novel techniques and approaches to enhance the fidelity of foraminiferal paleoclimate records (Doctoral Dissertation)*. Retrieved from ProQuest. (https://search.proquest.com/docview/2137634538). Madison, WI: Univ. of Wisconsin-Madison.

Wycech, J., Kelly, D. C., Kitajima, K., Kozdon, R., Orland, I. J., & Valley, J. W. (2018). Combined effects of gametogenic calcification and dissolution on δ^{18}O measurements of the planktic foraminifer *Trilobatus sacculifer*. *Geochemistry, Geophysics, Geosystems*, *18*, 1–15. https://doi.org/10.1029/2018GC007908

Wycech, J., Kelly, D. C., Kozdon, R., Orland, I. J., Spero, H. J., & Valley, J. W. (2018). Comparison of δ^{18}O analyses on individual planktic foraminifer (*Orbulina universa*) shells by SIMS and gas-source mass spectrometry. *Chemical Geology*, *483*, 119–130. https://doi.org/10.1016/j.chemgeo.2018.02.028

Wycech, J., Kelly, D. C., & Marcott, S. (2016). Effects of seafloor diagenesis on planktic foraminiferal radiocarbon ages. *Geology*, *44*, 551–554. https://doi.org/10.1130/G37864.1

Wycech, J. B., Gill, E. C., Rajagopalan, B., Marchitto, T. M. Jr., & Molnar, P. (2019). Multiproxy reduced-dimension reconstruction of Pliocene equatorial Pacific sea surface temperatures. *Paleoceanography and Paleoclimatology*, *35*, 1–20. https://doi.org/10.1029/2019PA003685

Xie, S. P. (2004). The shape of continents, air-sea interaction, and the rising branch of the Hadley Circulation. In H. F. Diaz, & R. S. Bradley (Eds.), *The Hadley circulation: Present, past and future* (pp. 121–152). Dordrecht: Springer.

Zeebe, R. E., & Tyrrell, T. (2019). History of carbonate ion concentration over the last 100 million years II: Revised calculations and new data. *Geochimica et Cosmochimica Acta*, *257*, 373–392. https://doi.org/10.1016/j.gca.2019.02.041

Zhang, X., Prange, M., Steph, S., Butzin, M., Krebs, U., Lunt, D. J., et al. (2012). Changes in equatorial Pacific thermocline depth in response to Panamanian seaway closure: Insights from a multi-model study. *Earth and Planetary Science Letters*, *317-318*, 76–84. https://doi.org/10.1016/j.epsl.2011.11.028

Zhang, Y. G., Pagani, M., & Liu, Z. (2014). A 12-million-year temperature history of the tropical Pacific Ocean. *Science*, *344*(6179), 84–87. https://doi.org/10.1126/science.1246172

Zhao, M., Hendon, H. H., Yin, Y., & Alves, O. (2016). Variations of upper-ocean salinity associated with ENSO from PEODAS reanalyses. *Journal of Climate*, *29*, 2077–2094. https://doi.org/10.1175/JCLI-D-15-0650.1

References From the Supporting Information

Ku, H. H. (1966). Notes on the use of propagation of error formulas. *Journal of Research of the National Bureau of Standards—C. Engineering and Instrumentation*, *70C*(4), 263–273. https://doi.org/10.6028/jres.070c.025